

The formation of a camalexin-biosynthetic metabolon

Stefanie Mucha^{a,b}, Stephanie Heinzlmeir^c, Verena Kriechbaumer^d, Benjamin Strickland^a, Charlotte Kirchhelle^{b, 2}, Manisha Choudhary^b, Natalie Kowalski^a, Ruth Eichmann^{e, 3}, Ralph Hückelhoven^e, Erwin Grill^a, Bernhard Küster^c, Erich Glawischnig^{a, b, f, 1}

^a Chair of Botany, Department of Plant Sciences, Technical University of Munich, Emil-Ramann-Str. 4, 85354 Freising, Germany.

^b Chair of Genetics, Department of Plant Sciences, Technical University of Munich, Emil-Ramann-Str. 8, 85354 Freising, Germany.

^c Chair of Proteomics and Bioanalytics, Technical University of Munich, Emil-Erlenmeyer-Forum 5, 85354 Freising, Germany.

^d Plant Cell Biology, Biological and Medical Sciences, Oxford Brookes University, Oxford, OX3 0BP, UK.

^e Chair of Phytopathology, Department of Plant Sciences, Technical University of Munich, Emil-Ramann-Str. 2, 85354 Freising, Germany.

^f Microbial Biotechnology, TUM Campus Straubing for Biotechnology and Sustainability, Technical University of Munich, Schulgasse 22, 94315 Straubing, Germany (present address).

¹ corresponding author, Email: Glawischnig@tum.de.

² present address: Department of Plant Sciences, University of Oxford, South Parks Road, Oxford OX1 3RB, UK

³ present address: School of Life Sciences, University of Warwick, Gibbet Hill Campus, Coventry, CV4 7AL, UK

ORCID IDs: 0000-0002-6382-7035 (S.M.); 0000-0002-1066-6565 (S.H.); 0000-0003-3782-5834 (V.K.); 0000-0002-1387-9013 (B.S.); 0000-0001-8448-6906 (C.K.); 0000-0001-8158-1318 (M.C.); 0000-0002-9464-6456 (N.K.); 0000-0002-9307-7773 (R.E.); 0000-0001-5632-5451 (R. H.); 0000-0003-4036-766X (E. Gr.); 0000-0002-9094-1677 (B.K.); 0000-0001-9280-5065 (E.Gl.)

Short title: The camalexin-biosynthetic metabolon

One-sentence summary: In *Arabidopsis thaliana*, the cytochrome P450 enzymes of the camalexin biosynthetic pathway form a metabolic complex to which the glutathione transferase U4 is recruited.

The author responsible for distribution of materials integral to the findings presented in this article in accordance with the policy described in the Instructions for Authors (www.plantcell.org) is: Erich Glawischnig (Glawischnig@tum.de).

Abstract

Arabidopsis thaliana efficiently synthesizes the antifungal phytoalexin camalexin without apparent release of bioactive intermediates, such as indole-3-acetaldoxime, suggesting channeling of the biosynthetic pathway by formation of an enzyme complex. To identify such protein interactions, two independent untargeted co-immunoprecipitation (co-IP) approaches with the biosynthetic enzymes CYP71B15 and CYP71A13 as baits were performed and the camalexin biosynthetic P450 enzymes were shown to co-purify. These interactions were confirmed by targeted co-IP and Förster resonance energy transfer measurements based on fluorescence lifetime microscopy (FRET-FLIM). Furthermore, interaction of CYP71A13 and *Arabidopsis* P450 Reductase 1 (ATR1) was observed. An increased substrate affinity of CYP79B2 in presence of CYP71A13 was shown, indicating allosteric interaction. Camalexin biosynthesis involves glutathionylation of an intermediary indole-3-cyanohydrin, synthesized by CYP71A12 and especially CYP71A13. It was demonstrated by FRET-FLIM and co-IP, that the glutathione transferase GSTU4, which is co-expressed with tryptophan- and camalexin-specific enzymes, was physically recruited to the complex. Surprisingly, camalexin concentrations were elevated in knock-out and reduced in *GSTU4* overexpressing plants. This shows that GSTU4 is not directly involved in camalexin biosynthesis but rather has a role in a competing mechanism.

Introduction

Cytochrome P450 enzymes are found in all domains of life, but are particularly diversified in plants. In *Arabidopsis thaliana*, 244 P450-encoding genes are annotated, and individual enzymes have been shown to play roles e.g. in the

69 biosynthesis of phytohormones or of compounds involved in defense (Bak et al.,
70 2011). However, the biological function of the vast majority of Arabidopsis P450
71 enzymes remains unclear. Typically, eukaryotic P450 enzymes are anchored to the
72 membrane of the endoplasmic reticulum (ER) with their catalytic centers facing the
73 cytosolic side. They are able to form homo- and heteromers (Reed and Backes,
74 2012) and there is growing evidence that these interactions have an effect on the
75 catalytic activities of the respective enzymes. This has been shown in detail for the
76 human enzymes CYP2E1, CYP3A4, and CYP3A5 (Davydov et al., 2015).

77 In contrast to human/animal systems, for plant P450 enzymes there is little
78 information on potential functional interactions. For CYP73A5 and CYP98A3,
79 physical interactions with each other and additional enzymes of the phenylpropanoid
80 biosynthetic pathway was demonstrated by co-purification and Förster resonance
81 energy transfer (FRET) (Bassard et al., 2012). Also for sporopollenin biosynthesis,
82 involving CYP703 and CYP704 isoforms, interactions with other pathway enzymes
83 have been demonstrated by pulldown, yeast-2-hybrid and FRET experiments
84 (Lallemant et al., 2013). Furthermore, there is evidence for complex formation of
85 flavonoid biosynthetic enzymes (Crosby et al., 2011; Dastmalchi et al., 2016).
86 Recently, it was shown in detail that the cyanogenic glucoside Dhurrin is synthesized
87 by a protein complex of two cytochrome P450 enzymes, a P450 reductase and a
88 glucosyl transferase (Laursen et al., 2016). These examples indicate formation of
89 transient enzyme complexes, also referred to as metabolons, allowing efficient
90 channeling of intermediates, in particular for the biosynthesis of secondary
91 metabolites (Fujino et al., 2018; Hawes and Kriechbaumer, 2018; Knudsen et al.,
92 2018).

93 In Arabidopsis, cytochrome P450 enzymes play a crucial role in the biosynthesis of
94 indolic defense compounds, such as indole glucosinolates, camalexin, 4-
95 hydroxyindole-3-carboxyl nitrile, or derivatives of indole-3-carboxylic acid (Rauhut
96 and Glawischnig, 2009; Sønderby et al., 2010; Böttcher et al., 2014; Rajniak et al.,
97 2015) (Fig. 1). For the biosynthesis of these specialized metabolites, tryptophan is
98 converted to indole-3-acetaldoxime (IAOx) by CYP79B2 and CYP79B3. *Cyp79b2*
99 *cyp79b3* double mutants, in which tryptophan-derived defense compounds are
100 essentially absent, have been shown to be significantly more susceptible to a variety
101 of pathogens (Zhao et al., 2002; Glawischnig et al., 2004; Böttcher et al., 2009;
102 Schlaeppli et al., 2010; Frerigmann et al., 2016). In healthy plants, IAOx is

predominantly oxidized by CYP83B1 (SUR2, RNT1) to the corresponding nitrile oxides or *aci*-nitro compound (Bak et al., 2001; Hansen et al., 2001), the precursors of indole glucosinolates. Pathogen infection or treatment with high dosages of UV light or heavy metals, such as silver nitrate, induce the production of CYP71A12 and CYP71A13, which in contrast dehydrate IAOx to indole-3-acetonitrile (IAN) in the biosynthesis of camalexin (Nafisi et al., 2007; Müller et al., 2015), which is the major metabolite synthesized in response to these stresses. In camalexin biosynthesis, IAN is then activated, presumably to indole cyanohydrin, which also involves CYP71A12 and CYP71A13, and conjugated with glutathione (Parisy et al., 2007) yielding GS-IAN. Glutathionylations are catalyzed by glutathione transferases (GSTs), which are found in all eukaryotes. Arabidopsis contains 54 GST genes belonging to 7 different classes (Krajewski et al., 2013). A number of GSTs have been shown to be capable of metabolizing xenobiotics (Dixon et al., 2002; Wagner et al., 2002), but with a few exceptions (Kitamura et al., 2004) the information on endogenous functions is limited, and it is unclear to which degree they are functionally redundant (Czerniawski and Bednarek, 2018). For GS-IAN formation, Su et al. (2011) suggested an involvement of GSTF6, which is a member of a small subfamily together with GSTF2, GSTF3 and GSTF7. Interestingly, camalexin concentrations detected in response to silver nitrate were not significantly different with respect to wildtype even in *gstf2 gstf3 gstf6* triple knockout mutants or a *gstf2 gstf3 gstf6 gstf7* knockdown line (Rauhut, 2009). This shows that alternative GSTs might also participate in this step. Subsequently, GS-IAN is shortened to Cys(IAN) involving gamma-glutamyl peptidase 1 (GGP1), and Cys(IAN) is then converted to camalexin by a unique bifunctional P450 enzyme, CYP71B15 (Fig. 1). *Cyp71b15* mutants (*phytoalexin deficient 3*, *pad3*) are camalexin-deficient and accumulate camalexin precursors, such as Cys(IAN), dihydrocamalexin acid (DHCA) and derivatives thereof (Glazebrook and Ausubel, 1994; Zhou et al., 1999; Bednarek et al., 2005; Schuhegger et al., 2006; Böttcher et al., 2009).

Despite camalexin being a major sink for tryptophan in response to various stresses, intermediates such as IAOx are not accumulating, suggesting possible metabolite channeling between interacting proteins. Therefore, we have hypothesized that camalexin is produced by a metabolon. In this work, we provide evidence that the cytochrome P450 enzymes of the camalexin biosynthetic pathway physically interact and we systematically analyzed the potential functions of GSTs in camalexin formation.

Results

Cellular and subcellular localization of CYP71B15

CYP71B15 was expressed as C-terminal GFP fusion protein under control of its own promoter. This construct was expressed in a *pad3* knockout mutant background and lines complementing the camalexin-deficient phenotype were selected. Expression of the CYP71B15-GFP protein was monitored by Western blot analysis and a line was selected for further analysis in which a strong GFP signal was observed in response to *Botrytis cinerea* infection, while the signal was absent in untreated leaves (Supplemental Figure 1A).

As a next step, we analyzed the cellular distribution and subcellular localization of CYP71B15-GFP in response to the fungal pathogens *B. cinerea*, *Alternaria brassicicola*, and *Erysiphe cruciferarum* (Fig. 2). In accordance with its biological function in phytoalexin biosynthesis, CYP71B15-GFP was only observed in cells in close proximity to successful pathogen infection. We observed a strong accumulation of CYP71B15-GFP around the site to *B. cinerea* infection (24 h after infection, hai) (Fig 2A-F), surrounding an area, where the necrotrophic fungus had apparently already started to macerate the leaf tissue and where no CYP71B15-GFP was detected, possibly because these cells were no longer metabolically active. For necrotrophic *A. brassicicola* (18 hai), CYP71B15-GFP expression, was only observed in cells in direct cellular contact with the fungus (Fig. 2G-L). In *E. cruciferarum* infected leaves (24 hai), highest CYP71B15-GFP abundance was observed in cells next to cells that had been attacked or penetrated by the biotrophic fungus (Fig. 2 M-R). Note that *E. cruciferarum* spores, which were not germinated, did not induce CYP71B15-GFP expression (Fig 2M-O). In all cases, CYP71B15-GFP was located in the ER, which also surrounds the nucleus. This is in accordance with the detected ER-localization in the heterologous *Nicotiana* system (see below). No focal protein accumulations at sites of plant-microbe interactions were detected.

Untargeted screen for interaction partners of CYP71B15

Applying this *CYP71B15_{pro}:CYP71B15-GFP* (*pad3*) line, an untargeted proteomics screen was set up to identify proteins which interact with CYP71B15 in *B. cinerea*-

infected, as model system for pathogen interactions, or in UV-irradiated plants. Rosette leaves of six weeks-old *CYP71B15_{pro}:CYP71B15-GFP* (*pad3*) and *pad3* plants were infected with *B. cinerea*. After 24 h, microsomes were prepared and solubilized. Co-IPs were performed and the eluates were subjected to trypsin digestion and MS analysis. An aliquot of starting material was also analyzed to determine the composition of microsomal proteins in response to *B. cinerea* infection. Along with the bait protein CYP71B15, which was the protein corresponding to the highest signal intensity, a total of 71 proteins significantly accumulated with respect to the control IPs. Strikingly, among these, 22 cytochrome P450 enzymes, e.g. CYP71B23, CYP84A1, and CYP706A1, were highly overrepresented (Fig. 3; Supplemental Figure 2A). CYP71A13, the enzyme channeling IAOx into the camalexin biosynthetic pathway, was among the interacting proteins which accumulated with highest intensity (average log₂ intensity = 25.4) and highest specificity (109-fold enrichment, p=0.00014). Interestingly, the P450 enzyme CYP83B1 which competes with camalexin-specific enzymes for the intermediate IAOx (Fig. 1) (Bak et al., 2001; Hansen et al., 2001), and CYP71B6 which is involved in IAN metabolism (Bak et al., 2001; Hansen et al., 2001; Böttcher et al., 2014; Müller et al., 2019), were also enriched. CYP71A12 was also significantly enriched with an Label-free quantification (LFQ) intensity approx. 12-fold lower than CYP71A13. CYP79B2 and ATR1 were detected in the co-IP, but the respective enrichments (4.5-fold, p=0.17 and 5.0-fold, p=0.022, respectively) were below the threshold of significance indicating weak or transient interaction with the observed CYP71B15-containing protein complex. Interestingly, PDR12/ABCG40, which was recently identified as camalexin transporter (He et al., 2019) was significantly enriched (7.8-fold; p=0.00029), indicating that biosynthesis and transport of camalexin to some extent might be physically linked. For a comprehensive overview of the proteomics data, see Supplemental Dataset 1.

To evaluate to which extent this result depends on the trigger of camalexin biosynthesis, IPs were also performed with UV-irradiated leaves. The general outcome was similar (Supplemental Figure 2B): Besides the bait, which showed highest abundance, P450 enzymes such as CYP71A13, CYP83B1 and CYP71B6 were highly enriched, but also CYP79B2 and CYP71A12 were co-purified with CYP71B15 (Supplemental Dataset 1).

Screen for inducible physical interactors of CYP71A13

CYP71A13 was consistently identified as interactor in an untargeted screen with CYP71B15 as bait. As a complementary approach, a CYP71A13-YFP fusion protein was expressed in Arabidopsis under control of the 35S promoter. Microsomes of UV-irradiated or untreated rosette leaves were isolated and solubilized, and a co-IP was performed to address (i) whether CYP71B15-CYP71A13 interaction is independent of the choice of baits, and (ii) which interaction partners specifically bind CYP71A13 in response to induction. A total of 875 proteins were reproducibly detected in the co-IPs of the UV-treated samples (Supplemental Dataset 2), including 26 cytochrome P450 enzymes, and the cytochrome P450 reductases ATR1 and ATR2. Constitutive expression of the bait allows to detect also binding partners under control conditions, where concentrations of CYP71A13 expressed under control of its native promoter are too low for quantitative work. As this approach can yield also unspecific binding partners, the analysis was focused on the differences of UV treatment versus control. Strikingly, only one protein, CYP71B15, was significantly enriched in the UV-treated versus the non-treated sample (Fig. 4). Five proteins were significantly depleted in the UV-treated versus the non-treated sample, including Nitrilase 3 (NIT3, approx. 7-fold), which has been suggested to convert IAN to the auxin indole-3-acetic acid (IAA) upon sulphur starvation (Kutz et al., 2002).

In summary, we conclude from the untargeted co-IP experiments that the core camalexin biosynthetic enzymes CYP71B15 and CYP71A13 physically interact with each other in challenged Arabidopsis rosette leaves. Also, CYP71B6 which specifically converts IAN to Indole-3-aldehyde (ICHO) and Indole-3-carboxylic acid (ICOOH) (Böttcher et al., 2014) was consistently identified as a member of the protein complex. In the untargeted screens, CYP79B2 was identified as binding partner of CYP71B15, although the specificity of this interaction was not significant. No interaction in an untargeted screen with CYP71A13 was observed. This indicates that binding of CYP79B2 to the proposed camalexin biosynthetic protein complex is weaker and more transient than the interaction between the camalexin-specific enzymes CYP71A13 and CYP71B15.

Physical interaction of camalexin biosynthetic enzymes is confirmed by targeted co-IP

In order to confirm the physical interaction of the camalexin biosynthetic enzymes CYP71A12, CYP71A13, CYP71B15 and ATR1, different combinations of these proteins were transiently expressed in *Nicotiana benthamiana* as C-terminally YFP- and FLAG-tagged proteins. Solubilized microsomes were applied to α -GFP-beads and IP and co-IP was monitored by Western Blot with GFP- and FLAG-specific antibodies, respectively (Fig. 5; Supplemental Figure 3). As negative controls, all proteins were additionally co-expressed with membrane-bound GFP in order to exclude protein interaction due to the YFP tag or unspecific binding of the FLAG tagged proteins to the polysaccharide chains of the GFP trap beads used for targeted co-IP. Interaction was shown for CYP71A13 with CYP71B15 and ATR1. CYP71B15 also interacts with CYP71A12. In addition, interaction of CYP71A13 and CYP71B15 with the glutathione transferase (GST) U4 (see below) was observed.

CLSM microscopy and FRET-FLIM analysis demonstrate physical interaction of biosynthetic enzymes *in vivo*

The subcellular localization of CYP71A12, CYP71A13, CYP71B15 and CYP79B2, as well as of GGP1 and the GSTs U2 and U4 (Fig. 6), was analyzed by confocal microscopy, three days after transient expression of corresponding C-terminal GFP- and RFP-fusion proteins in *N. benthamiana* (Fig. 6, Supplemental Figure 4). CYP71A12 (Supplemental Fig. 4A), CYP71A13 (Supplemental Fig. 4B), and CYP71B15 (Supplemental Fig. 4C) were localized to the ER and showed co-localization with the ER lumenal marker RFP-HDEL and with each other (Fig. 6 A-C, D-F). Interestingly, although all experimental conditions were chosen identical to the other P450 enzymes analyzed, CYP79B2-RFP expression was always weaker (Fig. 6G). Nevertheless, co-localization with CYP71A13 was observed (Fig. 6 I). Apparently, GGP1 was localized to the cytosol and to some extent mis-localization of CYP71A13 to the cytoplasm was induced by GGP1 co-expression (Fig. 6 J-L).

We analyzed physical interaction by FRET (Förster, 1948) measured by donor excited-state FLIM (Becker, 2012; Schoberer and Botchway, 2014). The reduction in the lifetime of the GFP (donor) fluorescence occurs only when an acceptor fluorophore (mRFP) is within a distance of 10 nm, indicating a very high proximity and most likely direct physical contact between the two proteins of interest. Fluorescence lifetime of CYP71A12-GFP (Fig. 7A), CYP71A13-GFP (Fig. 7B), and

CYP71B15-GFP (Fig. 7C) was quantified in combination with various potential binding partners. Interaction was shown for CYP71A12 with CYP71B15, CYP79B2, GSTU4 and the soluble camalexin-biosynthetic enzyme GGP1. CYP71A13 binds to CYP71A12, CYP71B15, CYP79B2, GSTU4, and GGP1. Furthermore, the fluorescence lifetime of CYP71B15-GFP in presence of CYP71A12, CYP79B2, GSTU4 or GGP1 was statistically significantly reduced, which indicates an interaction of also these enzymes.

Taking the co-IP and FRET-FLIM data together, essentially it was demonstrated that the known camalexin biosynthetic enzymes form a protein complex *in vivo*. Interestingly, no CYP71A12 or CYP71B15 homodimer formation was observed. This also demonstrates that e.g. the observed interactions between CYP71A12/A13 and CYP71B15 are not due to unspecific dimerization of the cytochrome P450s.

Enzymatic parameters of CYP79B2 indicate allosteric interaction with CYP71A13

In order to examine potential metabolic channeling, the first two pathway enzymes, CYP79B2 and CYP71A13 were co-expressed together with ATR1 in *Saccharomyces cerevisiae*. As a control, the CYP71A13 expression construct was replaced by an empty vector. Tryptophan-conversion by corresponding microsomes was monitored. A striking shift of the product spectrum towards formation of IAN was observed for CYP79B2/CYP71A13, with respect to CYP79B2/empty vector microsomes (Fig. 8A). In addition, co-expression of CYP79B2 and CYP71A13 reduced the apparent K_m -value of CYP79B2 for tryptophan more than two-fold ($6.9 \pm 0.9 \mu\text{M}$ versus $17.5 \pm 1.9 \mu\text{M}$) (Fig. 8B).

GSTU4 physically interacts with CYP71A13 and is relevant for the camalexin response

In camalexin biosynthesis, activated IAN, presumably indole cyanohydrin, is glutathionylated, probably involving a GST (Klein et al., 2013). The untargeted co-IP screens (Supplemental datasets 1 and 2) revealed only few GSTs as proteins co-purified with very low signal intensity. GSTF6, previously proposed to be involved in camalexin biosynthesis (Su et al., 2011) was not detected. Possibly the interaction of

the cytosolic GSTs with the P450 enzymes is not sufficiently strong to persist in presence of the applied Triton X-100 concentration. To evaluate which Arabidopsis GSTs are capable of this conversion, a qualitative screening was performed in a yeast strain in which four endogenous GSTs and three genes of glutathione conjugate catabolism were deleted (GTO1, GTO2, GTO3, TEF4, CPC, CPY, CIS2) (Krajewski et al., 2013; Kowalski, 2016) and in which expression plasmids for ATR1 and CYP71A13 were introduced. These yeast cells were transformed with each of the 54 Arabidopsis GSTs and after selection screened for biotransformation of IAN and glutathione yielding GS-IAN. When an empty vector was used instead of the CYP71A13 expression plasmid, no activity was detected. Also, when no Arabidopsis GST was expressed, no GS-IAN was synthesized. Strikingly, for 41 enzymes, including most of the phi- and tau-class GSTs, product formation was observed (Supplemental Figure 5). As an approach to identify which of the active GSTs is relevant *in planta*, transcriptomics data was surveyed for co-expression with camalexin biosynthetic genes. In particular, *GSTU4* is strongly induced by pathogens and correlated with the genes of camalexin biosynthesis (CYP71B15, $r=0.85$; CYP71A13 $r=0.77$, expression angler, *B. cinerea* set (Toufighi et al., 2005), see also Supplemental Table 1).

GSTU4 was co-expressed with CYP71A13 in *N. benthamiana* as RFP/GFP fusion proteins and their subcellular localization was monitored (Fig. 6; Supplemental Figure 4, 6). As control, *GSTU2* was included, which is closely related to *GSTU4* and a member of the same gene cluster, and only weakly transcriptionally co-regulated with genes of camalexin biosynthesis (CYP71B15, $r=0.53$, CYP71A13, $r=0.62$, expression angler (Toufighi et al., 2005), *B. cinerea* set). Physical interaction was tested for both pairs by FRET-FLIM. For *GSTU4*-RFP a strong reduction of the CYP71A12-GFP, CYP71A13-GFP and CYP71B15-GFP lifetimes was detected (Fig. 7). All three CYP71s and *GSTU2* did not physically interact (Fig. 7). Interaction of *GSTU4* with CYP71A13 and CYP71B15 was also demonstrated via co-IP analysis (Fig. 5)

To evaluate a potential function of *GSTU2* and *GSTU4* in camalexin biosynthesis, *gstu2* and *gstu4* knockout as well as *GSTU4* overexpression lines were analyzed for camalexin formation in response to UV-C light (Supplemental Figure 7A), silver nitrate treatment (Supplemental Figure 7B) and *B. cinerea* infection (Supplemental Figure 7C). While for *gstu2* no difference in camalexin levels relative to a wild-type control was observed, *gstu4* knockout mutants typically showed elevated camalexin

concentrations. Strikingly, in response to *B. cinerea* infection, *35S_{pro}:GSTU4* overexpression lines accumulated less camalexin than wildtype plants. To statistically evaluate these effects, data from four independent experiments were combined (Fig. 9). There is a significant negative effect of *GSTU4* on the relative camalexin concentration accumulating in response to *B. cinerea* infection.

Discussion

The physical interaction of enzymes is a powerful strategy to effectively channel biosynthetic pathways and avoid release of reactive intermediates. Upon induction, camalexin is a major sink for tryptophan. Nevertheless, intermediates such as IAOx are not accumulating, indicating metabolite channeling. Camalexin biosynthesis involves several P450 enzymes which are bound to ER membranes. Membrane anchoring restricts diffusion facilitating that P450 enzymes can serve as nuclei for the formation of metabolic complexes. In addition, the ER membrane can reorganize bringing cytochrome P450 enzymes into contact with pathway enzymes in other organelles, which was e.g. observed for CYP81F2 in the interaction of Arabidopsis with nonadapted powdery mildew *Blumeria graminis f. sp. hordei* (*Bgh*) (Fuchs et al., 2016). For the ultimate enzyme of the camalexin biosynthetic pathway, CYP71B15 (PAD3), in the interaction with *B. cinerea*, *A. brassicicola*, and *E. cruciferarum* (Fig. 2) we observed a strong induction of protein expression, but no focal accumulation. Highly localized expression at sites of interaction together with metabolic channeling in multienzyme complexes may ensure highly controlled and safe production of camalexin on demand.

We identified proteins which physically interact with CYP71B15 (PAD3) following an untargeted co-IP approach (Fig. 3). The relative abundance of the co-purified proteins do not reflect the relative protein abundance of the corresponding solubilized microsomes, which served as starting material. Based on LFQ intensities, P450 enzymes represent only a minor fraction of total microsomal proteins, whilst they are highly overrepresented in the co-IP samples and highly enriched with respect to control IPs. This shows that the interaction between CYP71B15 and other P450 enzymes is not random. CYP71A12 and CYP71A13 were co-purified with high significance, demonstrating the specific interaction of camalexin biosynthetic

enzymes. In addition, enzymes involved in other pathways, such as phenylpropanoid or glucosinolate metabolism, were also significantly enriched, including CYP71B6, which degrades IAN to ICOOH and cyanide. Remarkably, the detected CYP71B15-CYP73A5 and CYP71B15-CYP98A3 interactions were also observed in a reverse approach with the two phenylpropanoid biosynthetic enzymes as baits in a tandem affinity purification-based screen (Bassard et al., 2012). Possibly, direct or indirect interactions of CYP71B15 with P450 enzymes of other biosynthetic pathways involve mutual regulation of their catalytic activities. Alternatively, ER-bound P450s tend to interact as they are dependent on the reductases ATR1 or ATR2 (Bassard et al., 2012). However, these P450 reductases were detected in solubilized microsomes but not significantly enriched by co-IP. In addition, a number of membrane-bound kinases were enriched. Whether this interaction has a functional significance, e.g. by phosphorylation of the biosynthetic enzymes, remains to be investigated.

A second co-IP screen was performed with the aim to identify interacting proteins which are specifically inducible. Here, constitutively expressed CYP71A13 was used as a bait and UV-challenged leaves were compared with untreated controls (Fig. 4). Only one of the co-purified proteins was significantly enriched: CYP71B15. In conclusion, CYP71A13-CYP71B15 were robustly identified as a core protein complex and this interaction was confirmed by targeted co-IP and FRET-FLIM (Fig. 5, Fig. 7).

The formation of biosynthetic complexes is typically a transient and reversible process (Perkins et al., 2010). For targeted co-IP the bait and interacting proteins were transiently overexpressed, enabling also interactions with proteins of low abundance *in planta*. Here also a CYP71A13-ATR1 interaction was observed. Furthermore, interaction of CYP71A12-CYP79B2 and CYP71A13-CYP79B2 was revealed by FRET-FLIM analysis as this method is most suitable for detecting transient interaction of proteins. As co-IP experiments with microsomal proteins as baits involve solubilisation with mild detergents, cytosolic components of the complex will not directly be solubilized and therefore depleted relative to membrane bound partners. This is probably the case for GGP1, which was not enriched in the untargeted approaches. Similarly, a soluble GST has been proposed as component of the camalexin biosynthetic machinery, but apparently, no GSTs were significantly enriched in an untargeted co-IP with CYP71B15 as bait. For the detection of interactions between known membrane bound and soluble proteins, FRET-FLIM

analysis is powerful, as it is not affected by differences in protein solubility. Here, in addition to the interaction of the camalexin biosynthetic cytochrome P450 enzymes, we observed interaction of CYP71A13 with GSTU4 and GGP1 (Fig. 7).

Camalexin biosynthesis involves glutathionylation of IAN. As most *Arabidopsis* GSTs are capable of catalyzing this reaction *in vitro* in concert with CYP71A13 (Supplemental Figure 5), it can be postulated that function of a specific GST in camalexin biosynthesis is rather caused by its ability to interact with the biosynthetic machinery or local substrate concentration than by its substrate specificity. *GSTU4* is transcriptionally coregulated with camalexin and tryptophan biosynthetic genes and the corresponding protein was identified as physical interactor of CYP71A13 (Fig. 5, Fig. 7, Supplemental Table 1). Therefore, it was a prime candidate for being a key GST in camalexin biosynthesis. In contrast to this assumption, after infection with *B. cinerea*, *gstu4* knockout line had elevated concentrations of camalexin, whereas in overexpression plants, camalexin levels were reduced with respect to wild type leaves. This observation is opposite to the expectations for a camalexin biosynthetic gene. The mechanism by which GSTU4 negatively interferes with camalexin biosynthesis remains unclear. One possibility is that a subcellular transport process is involved, as some GSTs such as GSTF12 (TRANSPARENT TESTA 19), act as transporters between cellular compartments rather than as glutathione transferases (Kitamura et al., 2004; Sun et al., 2012). In this case, an intermediate of the biosynthesis could be exported from the metabolon and metabolized. Alternatively, GSTU4 could have a regulatory function. The human GST Pi acts as inhibitor of Jun N-terminal kinase (JNK). In response to UV irradiation or H₂O₂ treatment GSTp oligomerizes and dissociates from the GSTp–JNK complex (Adler et al., 1999). Whether such GST-dependent activation mechanism in response to stress is relevant also in *Arabidopsis* remains to be investigated. Also, it is unclear whether the interaction between P450/GSTU4 interaction is specific for the camalexin biosynthetic machinery or might play a more general role.

In conclusion, CYP79B2, CYP71A12/A13, CYP71B15, and ATR1 form a metabolic complex (Fig. 10). FRET-FLIM data indicated, that, in addition, GGP1 can be recruited to this complex. Based on the data of our untargeted co-IP screens ATR1 and CYP79B2 are likely to be less tightly associated with the core camalexin biosynthetic complex. This is in accordance with their different biological functions.

ATR1 is required for many different biosynthetic processes in *Arabidopsis*. CYP79B2 is also involved in the biosynthesis of indole glucosinolates (Hull et al., 2000; Mikkelsen et al., 2000), the biosynthesis of auxin under specific conditions (Brumos et al., 2014; Tivendale et al., 2014), and the remodeling of root architecture (Julkowska et al., 2017). A possible interaction of CYP79B2 with CYP83B1, which is involved in indole glucosinolate biosynthesis and competes with CYP71A12/A13 for IAOx, was not detected in co-IP and split-ubiquitin-based yeast 2-hybrid screens (Nintemann et al., 2017), potentially indicating a rather weak or temporary protein-protein binding. CYP79B2, a key branch-point enzyme being recruited for different processes is possibly modifying the activities of downstream enzymes. In yeast microsomes expressing CYP71A13 in addition to CYP79B2, the apparent binding constant for the substrate tryptophan was significantly reduced, indicating allosteric interaction and potentially substrate channeling. A similar effect was observed for the entry enzymes of flavonoid biosynthesis (Crosby et al., 2011). For other P450 enzymes of the pathway such an effect was not observed. However, they may require *Arabidopsis* components not present in the heterologous system. Substrate turnover numbers were not determined, as it is typically not possible to purify active membrane bound P450s to homogeneity (Cobbett et al., 1998). Therefore, the amount of mutual activation of catalytic activities might be underestimated and we hypothesize that the camalexin biosynthetic enzymes cooperatively interact to allow high flux to the end product.

Material and Methods

Plant growth conditions and stress treatment

After stratification for 2 days, *A. thaliana* and *N. benthamiana* plants were grown in a growth chamber under long-day conditions ($160 \mu\text{mol m}^{-2} \text{s}^{-1}$, 16 h light, 8 h dark) at 21°C and 50% relative humidity. For induction of phytoalexin biosynthesis *A. thaliana* 6-weeks-old rosette leaves were either sprayed with 5 mM AgNO_3 or treated with UV-C light for 2 h (Desaga UVVIS; $\lambda = 254 \text{ nm}$, 8 W, distance: 20 cm) or infected with *B. cinerea* spores (strain B05.10, 2×10^5 spores per ml). Camalexin was extracted after 24 h (UV-C and AgNO_3 treatment) or 48 h (*B. cinerea* infection).

Constructs for the expression of fusion proteins

For generation of CYP71B15-GFP under control of the endogenous promoter, the CYP71B15 promoter (Schuhegger et al., 2006; Chapman et al., 2016) was cloned into pBSK, and the CYP71B15 (At3g26830) CDS was introduced into this plasmid via NcoI/SmaI. The total insert was cut out by EcoRI/SmaI and introduced into pEVS-NL (Carnegie Institution). The promoter-CDS-GFP sequence was cut out with EcoRI/XbaI and introduced into the EcoRI/XbaI pGPTV-BarB vector fragment (Becker et al., 1992).

Constructs for YFP-, GFP-, RFP-, and FLAG-tagged proteins were created via the Gateway cloning system (Invitrogen™, Karimi et al. (2005), Katzen (2007)). Genes were amplified from *A. thaliana* cDNA with the listed primers (see below) and cloned into pDONR223. Plasmids were confirmed by sequencing. Based on this LR reaction was performed and constructs were transferred to the destination vectors which contains the 35S promoter and a tag (YFP: pEarlyGate101, GFP: pB7FWG2, RFP: pB7RWG2, FLAG: pEarlyGate202).

For cloning the following primers were used:

Gene	Primer (5'→3')
CYP71B15 (At3g26830)	GGGGACAAGTTTGTACAAAAAAGCAGGCTCTTATACTGTGGCT
	ATATATG
	GGGGACCACTTTGTACAAGAAAGCTGGGTTCCTTGCCCTGT
	TCTTGTG
CYP71A13 (At2g30770)	GGGGACAAGTTTGTACAAAAAAGCAGGCTTCATGAGCAATATT
	CAAGAAATGGA
	GGGGACCACTTTGTACAAGAAAGCTGGGTCTTCCACAACCGA
	AGATGGAAATG
CYP71A12 (At2g30750)	GGGGACAAGTTTGTACAAAAAAGCAGGCTTCATGAGCAATATT
	CAAGAAATGGA
	GGGGACCACTTTGTACAAGAAAGCTGGGTCTTGAATAACGGA
	AGATGGAAATGC
CYP79B2 (At4g39950)	GGGGACAAGTTTGTACAAAAAAGCAGGCTTCATGAACACTTTT
	AC

	GGGGACCACTTTGTACAAGAAAGCTGGGTCCCATCACTTCAC CGT
ATR1 (At4g24520)	GGGGACAAGTTTGTACAAAAAAGCAGGCTTCATGACTTCTGCT TTGTATGCTTCC
	GGGGACCACTTTGTACAAGAAAGCTGGGTCCTATCACCAGAC ATCTCTGAGGTATC
GSTU2 (At2g29480)	GGGGACAAGTTTGTACAAAAAAGCAGGCTTCATGGCGAAGAA AGAAGAGAGT
	GGGGACCACTTTGTACAAGAAAGCTGGGTCTTCGAACGTAGA CTTAGCTCT
GSTU4 (At2g29460)	GGGGACAAGTTTGTACAAAAAAGCAGGCTTCATGGCGGAGAA AGAAGAGGATGTG
	GGGGACCACTTTGTACAAGAAAGCTGGGTCTTCGGCTGATT GATTCTTTCTACC

482

483

484 Generation of transgenic *Arabidopsis* lines

485 *A. thaliana* accession Columbia was transformed with *Agrobacteria* harboring the
486 *CYP71B15_{pro}:CYP71B15-GFP* expression construct via floral dip (Clough and Bent,
487 1998). Phosphinothricin (PPT)-resistant primary transformants were confirmed by
488 PCR and qualitatively screened for GFP fluorescence in response to AgNO₃
489 spraying. A high-expression line was crossed to the *cyp71b15/pad3* T-DNA insertion
490 line SALK_026585 (Xu et al., 2008; Lemarié et al., 2015) and from the F2 generation
491 homozygous *pad3* / *CYP71B15_{pro}:CYP71B15-GFP* plants were selected which
492 carried the construct and, at least partially, complemented the camalexin-deficient
493 *pad3* phenotype (Supplemental Figure 1B). The progeny of one individual was used
494 for proteomics analysis. For constitutive expression of CYP71A13-YFP, a
495 corresponding pEarleyGate101 construct was used. Replicates represent
496 independent microsome preparations from independent plants.

497

498 Analysis of *CYP71B15-GFP* localization in response to pathogens

The *B. cinerea* strain B05.10 was cultivated on potato dextrose agar (PDA) under UV-light (12 h darkness, 12 h light) at RT. Preparation of *B. cinerea* spore suspension and inoculation procedure followed instructions in Gronover et al. (2001) using 10 µl droplets of a suspension of 8×10^5 conidia per ml on fully developed Arabidopsis leaves. *A. brassicicola* was grown on synthetic nutrient-poor agar (SNA, (Nirenberg, 1981) under UV-light. Fully developed Arabidopsis leaves were inoculated with 10 µl droplets of a suspension of 5×10^4 spores per ml H₂O / 0.02% (v/v) Tween20. Plants infected with *B. cinerea* or *A. brassicicola* were cultivated under normal growth conditions in a closed box in order to retain high humidity. For infection with *E. cruciferarum*, Arabidopsis plants were placed under an inoculation box covered with a polyamide net (0.2 mm²) and inoculated at a density of 3-5 conidia per mm² by brushing conidia off of powdery mildew infected plants. *E. cruciferarum* membranes were stained with 20 µM SynaptoRed™ C2 (also known as FM-464, Sigma-Aldrich) for 15 min in the dark. Images were taken with a confocal laser-scanning microscope (Leica SP5). GFP was excited with a 488 nm laser line and detected between 500 and 530 nm, SynaptoRed™ was excited at 561 nm and detected between 600 and 645 nm.

Transient expression in *Nicotiana benthamiana*

For transient protein expression in *Nicotiana benthamiana*, expression plasmids were transformed into *Agrobacterium tumefaciens* GV3101(MP90). Correct transformants were confirmed by PCR specific for the transgene. 25 ml overnight cultures were centrifuged and resuspended in 10 mM MES, 10 mM MgCl₂, 150 µM acetosyringone, pH=5.6 at an OD₆₀₀ of 0.5-0.6. The cells are then incubated in a shaker for 2 h (RT) and the cultures of *Agrobacterium* expressing the possibly interacting proteins and the supporting strain p19 were mixed in the ratio 1:1:1 (Sparkes et al., 2006). For each sample 4-6 leaves of *N. benthamiana* were infiltrated on the abaxial side of the leaves with a 1 ml syringe. After infiltration, before harvesting the infiltrated leaves, the plants were incubated for 3 d in a growth chamber under long-day conditions (160 µmol m⁻² s⁻¹, 16 h light, 8 h dark) at 21°C.

Plant microsome generation and co-immunoprecipitation

Infiltrated leaves were harvested and ground with a mix of sea sand and Polyklar® AT (Serva) (ratio 1:1) and 5 ml of ice-cold buffer 1 (100 mM ascorbic acid, 50 mM Na₂SO₄, 250 mM Tricin, 2 mM EDTA, DTE 2 mM, 5 g/L BSA, pH 8,2). 20 ml of buffer 1 was added and the homogenate was centrifuged (20,000xg, 4°C, 10 min). The supernatant was filtrated via a gauze bandage and centrifuged again. Microsomes were pelletized by centrifugation (60000xg, 4°C, 2 h) and in 1.5 ml buffer 2 (50 mM NaCl, 100 mM Tricin, 250 mM sucrose, 2 mM EDTA, 2 mM DTE, pH 8,2) resuspended.

For solubilisation, 500 µl microsomes were mixed with Triton X-100 to a final concentration of 0.5%. The samples are incubated at 4°C for 1 h under constant shaking and centrifuged (20000xg, 1.5 h, 4°C). The supernatant was transferred to a new Eppendorf tube and protein concentration determined photometrically (BIO-RAD Protein Assay).

For untargeted co-IP, GFP-Trap® A beads (Chromotek, Munich, Germany; Rothbauer et al. (2008)) were equilibrated with co-IP buffer (10 mM Tris; 150 mM NaCl; 0.5 mM EDTA) and mixed with 1 volume microsomes solubilized in 1% Triton X-100 (100 µl beads in a total volume of 4 ml for bait expressed under endogenous promoter, 50 µl beads / 2 ml for bait expressed under the 35S promoter). After incubation for 1 h at 4°C under constant shaking, beads were centrifuged (2700xg, 4°C, 2 min) and washed three times with co-IP buffer. The supernatant was replaced by 30 µl NuPAGE® LDS Sample Buffer (4x, Invitrogen GmbH, Karlsruhe, Germany) together with 30 µl 100 mM DTT and incubated at 70°C for 15 min. Targeted co-IP was performed with 10 µl GFP-Trap® A beads each, in a total volume of 500 µl. The samples were analyzed via western blot using anti-FLAG (Sigma, F1804) and anti-GFP (Invitrogen, A-11122) antibody followed by staining with goat anti-mouse HRP (Bio-Rad, 172-1011) or goat anti-rabbit HRP (Life Technologies, 65-6120) respectively (dilution of all antibodies 1:3000). Replicates represent independent microsome preparations from independent plants.

Protein identification by liquid chromatography and tandem mass spectrometry (LC-MS/MS)

In-gel digestion

Protein samples were reduced by 10 mM dithiothreitol, and alkylated by 55 mM iodoacetamide (CYP71B15 dataset) or 55 mM chloroacetamide (CYP71A13 dataset). Proteins were run into a 4–12% NuPAGE gel for about 1 cm to concentrate the sample prior to in-gel tryptic digestion. In-gel trypsin digestion was performed according to standard procedures (Shevchenko et al., 2006).

LC-MS/MS analysis of CYP71B15 experiments

Peptides generated by in-gel trypsin digestion were analyzed via LC-MS/MS on a nanoLC-Ultra 1D+ (Eksigent, Dublin, CA) coupled to an LTQ-Orbitrap Elite mass spectrometer (ThermoFisher Scientific). Peptides were delivered to a trap column (Reprosil-Pur C18 ODS3 5 μ m resin, Dr. Maisch, Ammerbuch, Germany, 20 mm \times 75 μ m, self-packed) at a flow rate of 5 μ l/min in 100% solvent A₀ (0.1% formic acid in HPLC grade water). Peptides were then transferred to an analytical column (Reprosil-Gold C18 120, 3 μ m, Dr. Maisch, Ammerbuch, Germany, 400 mm \times 75 μ m, self-packed) and separated using a 110 min gradient from 4% to 32% solvent B (0.1% formic acid and 5% DMSO in acetonitrile) in A (0.1% formic acid and 5% DMSO in HPLC grade water) at a flow rate of 300 nl/min. The mass spectrometer was operated in data dependent mode, automatically switching between MS and MS2 spectra. Up to 15 peptide precursors were subjected to fragmentation by higher energy collision-induced dissociation (HCD) and analyzed in the Orbitrap. Dynamic exclusion was set to 20 s.

LC-MS/MS analysis of CYP71A13 experiments

Peptides generated by in-gel trypsin digestion were analyzed via LC-MS/MS on a nanoLC-Ultra 1D+ (Eksigent, Dublin, CA) coupled to a Q Exactive HF mass spectrometer (ThermoFisher Scientific). Peptides were delivered to a trap column (75 μ m \times 2 cm, packed in house with Reprosil-Pur C18 ODS3 5 μ m resin, Dr. Maisch) for 10 min at a flow rate of 5 μ l/min in 100% solvent A₀ (0.1% formic acid in HPLC grade water). Peptides were then separated on an analytical column (75 μ m \times 40 cm, packed in-house with Reprosil-Gold C18 120, 3 μ m resin, Dr. Maisch) using a 120 min gradient ranging from 4-32% solvent B (0.1% formic acid and 5% DMSO in acetonitrile) in A (0.1% formic acid and 5% DMSO in HPLC grade water) at a flow rate of 300 nl/min. The mass spectrometer was operated in data dependent mode, automatically switching between MS and MS2 spectra. Up to 20 peptide precursors

were subjected to fragmentation by higher energy collision-induced dissociation (HCD) and analyzed in the Orbitrap. Dynamic exclusion was set to 20 s.

Peptide and protein identification and quantification

Label free quantification was performed using MaxQuant (version 1.6.1.0) (Cox and Mann, 2008) by searching MS data against an *Arabidopsis thaliana* reference database derived from UniProt (version 09.07.2016, 31424 entries) using the embedded search engine Andromeda (Cox et al., 2011). Carbamidomethylated cysteine was used as fixed modification; variable modifications included oxidation of methionine and N-terminal protein acetylation. Trypsin/P was specified as proteolytic enzyme with up to two allowed missed cleavage sites. Precursor tolerance was set to 10 ppm and fragment ion tolerance was set to 20 ppm. Label-free quantification (Cox et al., 2014), match-between-runs and intensity-based absolute quantification options were enabled and results were filtered for a minimal length of seven amino acids, 1% peptide and protein FDR as well as common contaminants and reverse identifications.

Data analysis and visualization

MaxQuant results were imported into the MaxQuant associated software suite Perseus (v.1.5.8.5) (Tyanova and Cox, 2018). Label-free quantification intensities (LFQ) were filtered for at least 3 valid values for at least one experimental group and at least 3 peptides for identification per protein. Missing values were imputed from normal distribution (width 0.2, downshift 2.0). A two-sided unpaired student's t-test was performed to assess statistical significance. Protein p-values were corrected for multiple testing using a permutation based 1% FDR cut-off (1000 permutations). Standard functions in the SAM R-package were used to adjust s_0 for each dataset (Tusher et al., 2001). For the CYP71B15 scatter plots proteins were filtered for at least 2 valid values for at least one experimental group and at least 3 peptides for identification per protein. Means were calculated and missing values were imputed by a constant (constant: 0).

Data deposition

Mass spectrometry data have been deposited to the ProteomeXchange Consortium (<http://proteomecentral.proteomexchange.org>) via the PRIDE partner repository (Vizcaíno et al., 2012) with the dataset identifier PXD008812 (reviewer account: username: reviewer70359@ebi.ac.uk, password: MRXOTnDO).

628

629 Yeast transformation, protein expression, yeast microsomes, enzyme analysis and
630 yeast feeding experiments

631 The *Saccharomyces cerevisiae* strain BY4741 (Brachmann et al., 1998), auxotroph
632 for His, Leu, Met and Ura, was used for coexpression of ATR1 (on plasmid
633 pGREG505), CYP79B2 (on plasmid pYeDP60) and CYP71A13 (on plasmid pSH62)
634 or the corresponding vector control. Transformations were performed according to
635 Gietz et al. (1992). Yeasts were cultivated and microsomes were prepared essentially
636 as described by (Schuhegger et al., 2006) , with the modification that instead of
637 SGIW medium the selection medium SD was used (Amberg et al., 2005).
638 Microsomes were resuspended in TEG buffer (50 mM Tris pH 7.5, 1 mM EDTA, 20%
639 glycerol, 2 mM DTE) and incubated with 0.5 mM NADPH and 5-200 μ M of tryptophan
640 for 45 to 90 min. To stop the reaction 2 Vol. of 100% methanol were added and the
641 reaction mix was centrifuged twice to remove macroscopic contaminants. The
642 conversion of tryptophan to indole-3-acetaldoxime was monitored by reverse-phase
643 HPLC (Lichrosphere 100 RP-18, 250 x 3 mm, 5 μ M, Merck; flow rate of 0.6 mL min-
644 1; solvents, 0.3% (v/v) formic acid in water (A) and acetonitrile (B); gradient: 0 to 2
645 min, isocratic, 25% B; 2 to 10.5 min, linear from 25% to 45% B; 10.5 to 13 min, linear
646 from 45% to 100% B; 13 to 15 min, isocratic, 100% B) and quantified based on a
647 calibration curve of the authentic standard (Glawischnig et al., 2004). Determination
648 of K_m values was performed via GraphPad PrismGraph (Michaelis-Menten analysis).

649 For feeding experiments yeasts carrying ATR1 (on plasmid pGREG505), CYP71A13
650 (on plasmid pYeDP60) and one out of 54 GSTs (on plasmid pSH62) were grown in
651 SD medium with appropriate supplements (-His, -Leu, -Met, -Ura) until $OD_{600} = 0.6$
652 was reached. Protein expression was induced by addition of galactose for 16 h.
653 Feeding was performed with 0.1 mM IAN and 0.2 mM GSH for 24 h. Subsequently
654 yeast cells were harvested, washed in ddH₂O, and 350 μ l methanol:formic acid;
655 99.8%:0.2% (v/v) was added. After vortexing and incubation at room temperature for
656 15 min under constant shaking cell debris were removed and GS-IAN formation
657 analyzed via HPLC (Lichrosphere 100 RP-18, 250 x 3 mm, 5 μ M, Merck; flow rate of
658 0.6 mL min-1; solvents, 0.3% (v/v) formic acid in water (A) and acetonitrile (B);
659 gradient: 0 to 2 min, isocratic, 25% B; 2 to 19 min, linear from 25% to 50% B; 19 to
660 24 min, linear from 50% to 100% B; 24 to 26 min, isocratic, 100% B), calibrating with

the authentic standard.

Confocal microscopy and FRET-FLIM analysis

For co-localization experiments leaf epidermal samples were imaged using a Zeiss PlanApo x100/1.46 NA oil immersion objective on a Zeiss LSM880 confocal equipped with an Airyscan detector. 512 × 512 images were collected in 8-bit with 2-line averaging at an (x,y) pixel spacing of 20–80 nm with excitation at 488 nm (GFP) and 561 nm (RFP), and emission at 495–550 nm and 570–615 nm, respectively. Data was produced from at least three independent biological replicates, defined as separate plants independently infiltrated from glycerol stocks. At least twenty cells per combination were imaged in a randomized manner.

FRET-FLIM analysis was performed according to Kriechbaumer et al. (2015). In brief: Epidermal samples of infiltrated leaves were excised and multiphoton FRET-FLIM data capture was performed by a two-photon microscope built around a Nikon TE2000-U inverted microscope with a modified Nikon EC2 confocal scanning system. Laser light at a wavelength of 920 nm was produced by a mode-locked titanium sapphire laser (Mira; Coherent Lasers), with 200-fs pulses at 76 MHz, pumped by a solid-state continuous wave 532-nm laser (Verdi V18; Coherent Laser). The laser beam was focused to a diffraction limited spot using a water-immersion objective (Nikon VC; 360, numerical aperture of 1.2). Fluorescence emission was collected bypassing the scanning system and passed through a BG39 (Comar) filter to block the near-infrared laser light. Line, frame, and pixel clock signals were generated and synchronized with an external detector in the form of a fast microchannel plate photomultiplier tube (Hamamatsu R3809U). Raw FRET-FLIM data was generated by linking these via a time-correlated single-photon counting PC module SPC830 (Becker and Hickl). Prior to FLIM data collection, the GFP and mRFP expression levels in the plant samples within the region of interest were confirmed using a Nikon EC2 confocal microscope with excitation at 488 and 543 nm, respectively. A 633-nm interference filter is used to significantly minimize the contaminating effect of chlorophyll autofluorescence emission.

Data were analyzed by obtaining excited-state lifetime values first on a pixel by pixel basis, then of a region of interest on the nuclear envelope, and calculations were made using SPCImage analysis software version 5.1. The distribution of lifetime

values within the region of interest was generated and displayed as a curve. Only values with a χ^2 between 0.9 and 1.4 were considered. The median lifetime, minimum and maximum values for one-quarter of the median lifetime values from the curve were taken to generate the range of lifetimes per sample. Data from a minimum of three independent biological replicas and at least five nuclei per replica and per protein-protein combination were analyzed, and the average of the ranges was taken. Biological replicas are defined as separate plants independently infiltrated and analyzed.

Camalexin extraction

Camalexin extraction was performed according to (Müller et al., 2015). In brief, leaves were weighed and 400 µl of methanol:water (80:20, v/v) was added. After incubation for 1 h at 65°C under constant shaking, extracts were cleaned twice via centrifugation and analyses by reverse-phase HPLC (MultoHigh 100 RP18, 5-mm particle size; Göhler Analytik).

Acknowledgements

We thank Alfons Gierl for hosting the Glawischnig lab during the early phase of the project, Thomas Rauhut for generation the CYP71B15-GFP construct, Vasko Veljanovski for generation of CYP79B2 and GGP1 expression constructs, Alexandra Chapman, Verena Stork, and Marion Lechner for supporting co-IP establishment and generation of yeast strains, respectively, Aaron Klepper for providing homozygous *gstu4* T-DNA-lines, Ramón Torres Ruiz (CALM) for supporting FRET-FLIM instrument handling, and Danièle Werck for providing CYP73A5-YFP construct as negative control.

This work has been supported by the Deutsche Forschungsgemeinschaft, grants GL346/5 (DFG Heisenberg Fellowship to Erich Glawischnig) and GL346/8, the Hans-Fischer-Gesellschaft e.V., the TUM Junior Fellow Fund and a Science and Technology Facilities Council Program (FRET-FLIM grant no. 14230008).

Author contributions

S.M. designed and conducted the majority of experiments; S.H. performed proteomics analysis under the guidance of B.K.; V.K. performed FRET-FLIM and colocalization studies; B.S. and E.Gl. performed P450 expression in yeast; C.K. and M.C. generated lines for untargeted co-IP; M.C. and E.Gl. performed untargeted co-IP; N.K., under the guidance of E.Gr., generated yeast strains expressing GSTs; R. E. performed confocal microscopic analysis of pathogen infected material under the guidance of R. H.. E. Gl. designed and supervised the overall project; E.Gl. and S.M. wrote the article with contributions of all authors.

Figure Legends

Fig.1: Biosynthetic pathway of camalexin and related metabolites

Fig.2: CYP71B15-GFP accumulates in cells surrounding fungal infection sites

Fig. 3: Proteins co-purified with CYP71B15-GFP from leaves infected with *B. cinerea*

Fig. 4: Proteins co-purified from leaves overexpressing CYP71A13 with or without UV irradiation

Fig. 5: Co-IP analysis of the physical association of camalexin-specific enzymes

Fig. 6: Co-localization of camalexin-specific enzymes in *N. benthamiana* leaves

Fig. 7: Tight physical interaction of camalexin-biosynthesis enzymes supported by Förster Resonance Energy Transfer studies combined with Fluorescence Life Time Microscopy (FRET-FLIM)

Fig. 8: Higher apparent substrate affinity of CYP79B2 by presence of CYP71A13

Fig. 9: Camalexin formation in response to *B. cinerea* infection in *gstu4* knockout and overexpression plants

Fig. 10: Model of a camalexin-biosynthetic metabolon

759 References

- 760 **Adler, V., Yin, Z., Fuchs, S.Y., Benezra, M., Rosario, L., Tew, K.D., Pincus, M.R., Sardana, M.,**
761 **Henderson, C.J., and Wolf, C.R.** (1999). Regulation of JNK signaling by GSTp. *The EMBO journal* **18**, 1321-
762 1334.
- 763 **Amberg, D.C., Burke, D.J., and Strathern, J.N.** (2005). *Methods in Yeast Genetics: A Cold Spring Harbor*
764 *Laboratory Course Manual*, 2005 Edition (Cold Spring).
- 765 **Bak, S., Tax, F.E., Feldmann, K.A., Galbraith, D.W., and Feyereisen, R.** (2001). CYP83B1, a cytochrome
766 P450 at the metabolic branch point in auxin and indole glucosinolate biosynthesis in *Arabidopsis*. *The*
767 *Plant Cell* **13**, 101-111.
- 768 **Bak, S., Beisson, F., Bishop, G., Hamberger, B., Höfer, R., Paquette, S., and Werck-Reichhart, D.**
769 (2011). Cytochromes P450. *The Arabidopsis Book*, e0144.
- 770 **Bassard, J.E., Richert, L., Geerinck, J., Renault, H., Duval, F., Ullmann, P., Schmitt, M., Meyer, E.,**
771 **Mutterer, J., Boerjan, W., De Jaeger, G., Mely, Y., Goossens, A., and Werck-Reichhart, D.** (2012).
772 Protein-protein and protein-membrane associations in the lignin pathway. *Plant Cell* **24**, 4465-4482.
- 773 **Becker, D., Kemper, E., Schell, J., and Masterson, R.** (1992). New plant binary vectors with selectable
774 markers located proximal to the left T-DNA border. *Plant Molecular Biology* **20**, 1195-1197.
- 775 **Becker, W.** (2012). Fluorescence lifetime imaging-techniques and applications. *Journal of Microscopy*
776 **247**, 119-136.
- 777 **Bednarek, P., Schneider, B., Svatoš, A., Oldham, N.J., and Hahlbrock, K.** (2005). Structural complexity,
778 differential response to infection, and tissue specificity of indolic and phenylpropanoid secondary
779 metabolism in *Arabidopsis* roots. *Plant Physiology* **138**, 1058-1070.
- 780 **Böttcher, C., Westphal, L., Schmotz, C., Prade, E., Scheel, D., and Glawischnig, E.** (2009). The
781 multifunctional enzyme CYP71B15 (PHYTOALEXIN DEFICIENT3) converts cysteine-indole-3-acetonitrile
782 to camalexin in the indole-3-acetonitrile metabolic network of *Arabidopsis thaliana*. *Plant Cell* **21**, 1830-
783 1845.
- 784 **Böttcher, C., Chapman, A., Fellermeier, F., Choudhary, M., Scheel, D., and Glawischnig, E.** (2014). The
785 Biosynthetic Pathway of Indole-3-Carbaldehyde and Indole-3-Carboxylic Acid Derivatives in *Arabidopsis*.
786 *Plant Physiol* **165**, 841-853.
- 787 **Brachmann, C.B., Davies, A., Cost, G.J., Caputo, E., Li, J., Hieter, P., and Boeke, J.D.** (1998). Designer
788 deletion strains derived from *Saccharomyces cerevisiae* S288C: a useful set of strains and plasmids for
789 PCR-mediated gene disruption and other applications. *Yeast* **14**, 115-132.
- 790 **Brumos, J., Alonso, J.M., and Stepanova, A.N.** (2014). Genetic aspects of auxin biosynthesis and its
791 regulation. *Physiologia Plantarum* **151**, 3-12.
- 792 **Chapman, A., Lindermayr, C., and Glawischnig, E.** (2016). Expression of antimicrobial peptides under
793 control of a camalexin-biosynthetic promoter confers enhanced resistance against *Pseudomonas syringae*.
794 *Phytochemistry* **122**, 76-80.
- 795 **Clough, S.J., and Bent, A.F.** (1998). Floral dip: a simplified method for *Agrobacterium*-mediated
796 transformation of *Arabidopsis thaliana*. *Plant Journal* **16**, 735-743.
- 797 **Cobbett, C.S., May, M.J., Howden, R., and Rolls, B.** (1998). The glutathione-deficient, cadmium-sensitive
798 mutant, *cad2-1*, of *Arabidopsis thaliana* is deficient in gamma-glutamylcysteine synthetase. *Plant J* **16**, 73-
799 78.
- 800 **Cox, J., and Mann, M.** (2008). MaxQuant enables high peptide identification rates, individualized ppb-
801 range mass accuracies and proteome-wide protein quantification. *Nature Biotechnology* **26**, 1367.
- 802 **Cox, J., Neuhauser, N., Michalski, A., Scheltema, R.A., Olsen, J.V., and Mann, M.** (2011). Andromeda: a
803 peptide search engine integrated into the MaxQuant environment. *Journal of Proteome Research* **10**,
804 1794-1805.
- 805 **Cox, J., Hein, M.Y., Lubner, C.A., Paron, I., Nagaraj, N., and Mann, M.** (2014). Accurate Proteome-wide
806 Label-free Quantification by Delayed Normalization and Maximal Peptide Ratio Extraction, Termed
807 MaxLFQ. *Molecular & Cellular Proteomics* **13**, 2513-2526.
- 808 **Crosby, K.C., Pietraszewska-Bogiel, A., Gadella, T.W., Jr., and Winkel, B.S.** (2011). Forster resonance
809 energy transfer demonstrates a flavonoid metabolon in living plant cells that displays competitive
810 interactions between enzymes. *FEBS Letters* **585**, 2193-2198.
- 811 **Czerniawski, P., and Bednarek, P.** (2018). Glutathione S-Transferases in the Biosynthesis of Sulfur-
812 Containing Secondary Metabolites in Brassicaceae Plants. *Front Plant Sci* **9**, 1639.
- 813 **Dastmalchi, M., Bernards, M.A., and Dhaubhadel, S.** (2016). Twin anchors of the soybean isoflavonoid
814 metabolon: evidence for tethering of the complex to the endoplasmic reticulum by IFS and C4H. *The Plant*
815 *Journal* **85**, 689-706.

Davydov, D.R., Davydova, N.Y., Sineva, E.V., and Halpert, J.R. (2015). Interactions among cytochromes P450 in microsomal membranes: oligomerization of cytochromes P450 3A4, 3A5, and 2E1 and its functional consequences. *Journal of Biological Chemistry* **290**, 3850-3864.

Dixon, D.P., Laphorn, A., and Edwards, R. (2002). Plant glutathione transferases. *Genome Biology* **3**, reviews3004. 3001.

Förster, T. (1948). Zwischenmolekulare Energiewanderung und Fluoreszenz. *Annalen der Physik* **437**, 55-75.

Frerigmann, H., Pislewska-Bednarek, M., Sanchez-Vallet, A., Molina, A., Glawischnig, E., Gigolashvili, T., and Bednarek, P. (2016). Regulation of Pathogen-Triggered Tryptophan Metabolism in *Arabidopsis thaliana* by MYB Transcription Factors and Indole Glucosinolate Conversion Products. *Mol Plant* **9**, 682-695.

Fuchs, R., Kopischke, M., Klapprodt, C., Hause, G., Meyer, A.J., Schwarzlander, M., Fricker, M.D., and Lipka, V. (2016). Immobilized Subpopulations of Leaf Epidermal Mitochondria Mediate PENETRATION2-Dependent Pathogen Entry Control in *Arabidopsis*. *The Plant cell* **28**, 130-145.

Fujino, N., Tenma, N., Waki, T., Ito, K., Komatsuzaki, Y., Sugiyama, K., Yamazaki, T., Yoshida, S., Hatayama, M., Yamashita, S., Tanaka, Y., Motohashi, R., Denessiouk, K., Takahashi, S., and Nakayama, T. (2018). Physical interactions among flavonoid enzymes in snapdragon and torenia reveal the diversity in the flavonoid metabolon organization of different plant species. *Plant J* **94**, 372-392.

Gietz, D., St Jean, A., Woods, R.A., and Schiestl, R.H. (1992). Improved method for high efficiency transformation of intact yeast cells. *Nucleic Acids Research* **20**, 1425.

Glawischnig, E., Hansen, B.G., Olsen, C.E., and Halkier, B.A. (2004). Camalexin is synthesized from indole-3-acetaldoxime, a key branching point between primary and secondary metabolism in *Arabidopsis*. *Proceedings of the National Academy of Sciences* **101**, 8245-8250.

Glazebrook, J., and Ausubel, F.M. (1994). Isolation of phytoalexin-deficient mutants of *Arabidopsis thaliana* and characterization of their interactions with bacterial pathogens. *Proceedings of the National Academy of Sciences* **91**, 8955-8959.

Gronover, C.S., Kasulke, D., Tudzynski, P., and Tudzynski, B. (2001). The role of G protein alpha subunits in the infection process of the gray mold fungus *Botrytis cinerea*. *Mol Plant Microbe Interact* **14**, 1293-1302.

Hansen, C.H., Du, L., Naur, P., Olsen, C.E., Axelsen, K.B., Hick, A.J., Pickett, J.A., and Halkier, B.A. (2001). CYP83B1 is the oxime-metabolizing enzyme in the glucosinolate pathway in *Arabidopsis*. *Journal of Biological Chemistry* **276**, 24790-24796.

Hawes, C., and Kriechbaumer, V. (2018). *The Plant Endoplasmic Reticulum*. (Springer).

He, Y., Xu, J., Wang, X., He, X., Wang, Y., Zhou, J., Zhang, S., and Meng, X. (2019). The *Arabidopsis* Pleiotropic Drug Resistance Transporters PEN3 and PDR12 Mediate Camalexin Secretion for Resistance to *Botrytis cinerea*. *The Plant cell*.

Julkowska, M., Koevoets, I.T., Mol, S., Hoefsloot, H.C., Feron, R., Tester, M., Keurentjes, J.J., Korte, A., Haring, M.A., and de Boer, G.-J. (2017). Genetic Components of Root Architecture Remodeling in Response to Salt Stress. *The Plant Cell*, tpc. 00680.02016.

Karimi, M., De Meyer, B., and Hilson, P. (2005). Modular cloning in plant cells. *Trends in Plant Science* **10**, 103-105.

Katzen, F. (2007). Gateway® recombinational cloning: a biological operating system. *Expert Opinion on Drug Discovery* **2**, 571-589.

Kitamura, S., Shikazono, N., and Tanaka, A. (2004). TRANSPARENT TESTA 19 is involved in the accumulation of both anthocyanins and proanthocyanidins in *Arabidopsis*. *The Plant Journal* **37**, 104-114.

Klein, A.P., Anarat-Cappillino, G., and Sattely, E.S. (2013). Minimum Set of Cytochromes P450 for Reconstituting the Biosynthesis of Camalexin, a Major *Arabidopsis* Antibiotic. *Angewandte Chemie International Edition* **52**, 13625-13628.

Knudsen, C., Gallage, N.J., Hansen, C.C., Moller, B.L., and Laursen, T. (2018). Dynamic metabolic solutions to the sessile life style of plants. *Nat Prod Rep* **35**, 1140-1155.

Kowalski, N.A. (2016). Charakterisierung der Glutathiontransferasen aus *Arabidopsis thaliana*. In Fakultät Wissenschaftszentrum Weihenstephan (Freising: TU-München), pp. 216.

Krajewski, M.P., Kanawati, B., Fekete, A., Kowalski, N., Schmitt-Kopplin, P., and Grill, E. (2013). Analysis of *Arabidopsis* glutathione-transferases in yeast. *Phytochemistry* **91**, 198-207.

Kriechbaumer, V., Botchway, S.W., Slade, S.E., Knox, K., Frigerio, L., Oparka, K., and Hawes, C. (2015). Reticulomics: Protein-Protein Interaction Studies with Two Plasmodesmata-Localized Reticulon Family Proteins Identify Binding Partners Enriched at Plasmodesmata, Endoplasmic Reticulum, and the Plasma Membrane. *Plant Physiology* **169**, 1933-1945.

Kutz, A., Müller, A., Hennig, P., Kaiser, W.M., Piotrowski, M., and Weiler, E.W. (2002). A role for nitrilase 3 in the regulation of root morphology in sulphur-starving *Arabidopsis thaliana*. *The Plant Journal* **30**, 95-106.

Lallemant, B., Erhardt, M., Heitz, T., and Legrand, M. (2013). Sporopollenin biosynthetic enzymes interact and constitute a metabolon localized to the endoplasmic reticulum of tapetum cells. *Plant physiology* **162**, 616-625.

Laursen, T., Borch, J., Knudsen, C., Bavishi, K., Torta, F., Martens, H.J., Silvestro, D., Hatzakis, N.S., Wenk, M.R., and Dafforn, T.R. (2016). Characterization of a dynamic metabolon producing the defense compound dhurrin in sorghum. *Science* **354**, 890-893.

Lemarié, S., Robert-Seilanian, A., Lariagon, C., Lemoine, J., Marnet, N., Levrel, A., Jubault, M., Manzaneres-Dauleux, M.J., and Gravot, A. (2015). Camalexin contributes to the partial resistance of *Arabidopsis thaliana* to the biotrophic soilborne protist *Plasmodiophora brassicae*. *Frontiers in plant science* **6**.

Mikkelsen, M.D., Hansen, C.H., Wittstock, U., and Halkier, B.A. (2000). Cytochrome P450 CYP79B2 from *Arabidopsis* catalyzes the conversion of tryptophan to indole-3-acetaldoxime, a precursor of indole glucosinolates and indole-3-acetic acid. *Journal of Biological Chemistry* **275**, 33712-33717.

Müller, T.M., Böttcher, C., and Glawischnig, E. (2019). Dissection of the network of indolic defence compounds in *Arabidopsis thaliana* by multiple mutant analysis. *Phytochemistry* **161**, 11-20.

Müller, T.M., Böttcher, C., Morbitzer, R., Götz, C.C., Lehmann, J., Lahaye, T., and Glawischnig, E. (2015). Transcription activator-like effector nuclease-mediated generation and metabolic analysis of camalexin-deficient *cyp71a12 cyp71a13* double knockout lines. *Plant Physiology* **168**, 849-858.

Nafisi, M., Goregaoker, S., Botanga, C.J., Glawischnig, E., Olsen, C.E., Halkier, B.A., and Glazebrook, J. (2007). *Arabidopsis* cytochrome P450 monooxygenase 71A13 catalyzes the conversion of indole-3-acetaldoxime in camalexin synthesis. *The Plant cell* **19**, 2039-2052.

Nintemann, S.J., Vik, D., Svozil, J., Bak, M., Baerenfaller, K., Burow, M., and Halkier, B.A. (2017). Unravelling protein-protein interaction networks linked to aliphatic and indole glucosinolate biosynthetic pathways in *Arabidopsis*. *Frontiers in Plant Science* **8**.

Nirenberg, H.I. (1981). A simplified method for identifying *Fusarium* spp. occurring on wheat. *Canadian Journal of Botany* **59**, 1599-1609.

Parisy, V., Poinssot, B., Owsianowski, L., Buchala, A., Glazebrook, J., and Mauch, F. (2007). Identification of PAD2 as a γ -glutamylcysteine synthetase highlights the importance of glutathione in disease resistance of *Arabidopsis*. *The Plant Journal* **49**, 159-172.

Perkins, J.R., Diboun, I., Dessailly, B.H., Lees, J.G., and Orengo, C. (2010). Transient protein-protein interactions: structural, functional, and network properties. *Structure* **18**, 1233-1243.

Rajniak, J., Barco, B., Clay, N.K., and Sattely, E.S. (2015). A new cyanogenic metabolite in *Arabidopsis* required for inducible pathogen defence. *Nature* **525**, 376-379.

Rauhut, T. (2009). Die Regulation der Camalexinbiosynthese in *Arabidopsis thaliana*. In *Lehrstuhl für Genetik* (Freising: TU-München).

Rauhut, T., and Glawischnig, E. (2009). Evolution of camalexin and structurally related indolic compounds. *Phytochemistry* **70**, 1638-1644.

Reed, J.R., and Backes, W.L. (2012). Formation of P450·P450 complexes and their effect on P450 function. *Pharmacology & Therapeutics* **133**, 299-310.

Rothbauer, U., Zolghadr, K., Muyldermans, S., Schepers, A., Cardoso, M.C., and Leonhardt, H. (2008). A versatile nanotrap for biochemical and functional studies with fluorescent fusion proteins. *Molecular & Cellular Proteomics* **7**, 282-289.

Schlaeppli, K., Abou-Mansour, E., Buchala, A., and Mauch, F. (2010). Disease resistance of *Arabidopsis* to *Phytophthora brassicae* is established by the sequential action of indole glucosinolates and camalexin. *The Plant Journal* **62**, 840-851.

Schoberer, J., and Botchway, S.W. (2014). Investigating protein-protein interactions in the plant endomembrane system using multiphoton-induced FRET-FLIM. *Methods in Molecular Biology* **1209**, 81-95.

Schuhegger, R., Nafisi, M., Mansourova, M., Petersen, B.L., Olsen, C.E., Svatos, A., Halkier, B.A., and Glawischnig, E. (2006). CYP71B15 (PAD3) catalyzes the final step in camalexin biosynthesis. *Plant Physiology* **141**, 1248-1254.

Shevchenko, A., Tomas, H., Havli, J., Olsen, J.V., and Mann, M. (2006). In-gel digestion for mass spectrometric characterization of proteins and proteomes. *Nature Protocols* **1**, 2856.

Sønderby, I.E., Geu-Flores, F., and Halkier, B.A. (2010). Biosynthesis of glucosinolates—gene discovery and beyond. *Trends in plant science* **15**, 283-290.

Sparkes, I.A., Runions, J., Kearns, A., and Hawes, C. (2006). Rapid, transient expression of fluorescent fusion proteins in tobacco plants and generation of stably transformed plants. *Nature Protocols* **1**, 2019-2025.

Su, T.B., Xu, J.A., Li, Y.A., Lei, L., Zhao, L., Yang, H.L., Feng, J.D., Liu, G.Q., and Ren, D.T. (2011). Glutathione-Indole-3-Acetonitrile Is Required for Camalexin Biosynthesis in *Arabidopsis thaliana*. *Plant Cell* **23**, 364-380.

Sun, Y., Li, H., and Huang, J.-R. (2012). Arabidopsis TT19 Functions as a Carrier to Transport Anthocyanin from the Cytosol to Tonoplasts. *Molecular Plant* **5**, 387-400.

Tivendale, N.D., Ross, J.J., and Cohen, J.D. (2014). The shifting paradigms of auxin biosynthesis. *Trends in Plant Science* **19**, 44-51.

Toufighi, K., Brady, S.M., Austin, R., Ly, E., and Provart, N.J. (2005). The botany array resource: e-northerns, expression angling, and promoter analyses. *The Plant Journal* **43**, 153-163.

Tusher, V.G., Tibshirani, R., and Chu, G. (2001). Significance analysis of microarrays applied to the ionizing radiation response. *Proceedings of the National Academy of Sciences* **98**, 5116-5121.

Tyanova, S., and Cox, J. (2018). Perseus: A Bioinformatics Platform for Integrative Analysis of Proteomics Data in Cancer Research. In *Cancer Systems Biology* (Springer), pp. 133-148.

Vizcaíno, J.A., Côté, R.G., Csordas, A., Dianes, J.A., Fabregat, A., Foster, J.M., Griss, J., Alpi, E., Birim, M., and Contell, J. (2012). The PRoteomics IDentifications (PRIDE) database and associated tools: status in 2013. *Nucleic Acids Research* **41**, D1063-D1069.

Wagner, U., Edwards, R., Dixon, D.P., and Mauch, F. (2002). Probing the diversity of the Arabidopsis glutathione S-transferase gene family. *Plant Molecular Biology* **49**, 515-532.

Xu, J., Li, Y., Wang, Y., Liu, H., Lei, L., Yang, H., Liu, G., and Ren, D. (2008). Activation of MAPK kinase 9 induces ethylene and camalexin biosynthesis and enhances sensitivity to salt stress in Arabidopsis. *Journal of Biological Chemistry* **283**, 26996-27006.

Zhao, Y., Hull, A.K., Gupta, N.R., Goss, K.A., Alonso, J., Ecker, J.R., Normanly, J., Chory, J., and Celenza, J.L. (2002). Trp-dependent auxin biosynthesis in Arabidopsis: involvement of cytochrome P450s CYP79B2 and CYP79B3. *Genes & Development* **16**, 3100-3112.

Zhou, N., Tootle, T.L., and Glazebrook, J. (1999). Arabidopsis PAD3, a gene required for camalexin biosynthesis, encodes a putative cytochrome P450 monooxygenase. *The Plant Cell* **11**, 2419-2428.

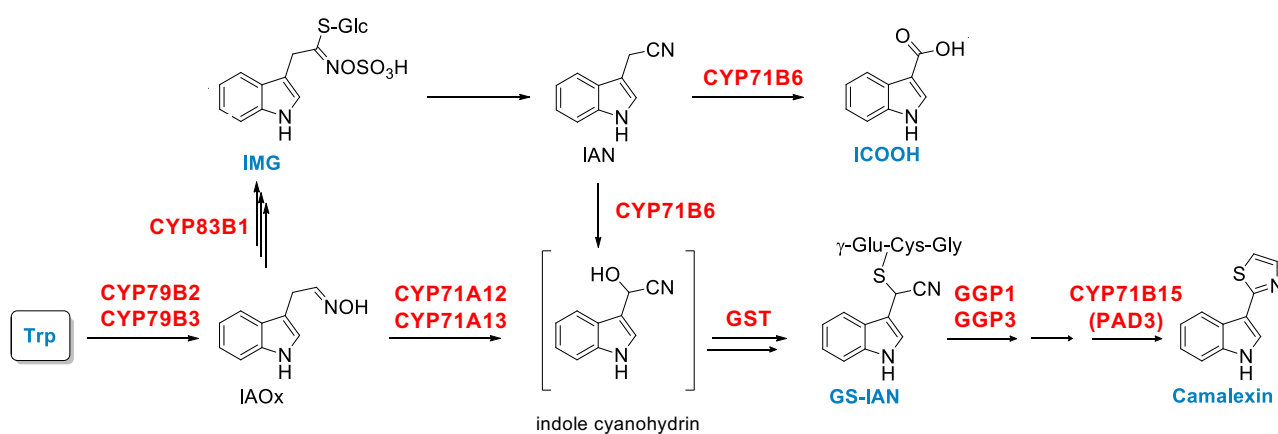


Figure 1: Biosynthetic pathway of camalexin and related metabolites

Enzymes are marked in red, detected compounds are labeled in blue and biosynthetic intermediates in black; IMG: indole-3-methylglucosinolate; IAOx: indole-3-acetaldoxime; IAN: indole-3-acetonitrile; GS-IAN: IAN glutathione conjugate; ICOOH: indole-3-carboxylic acid.

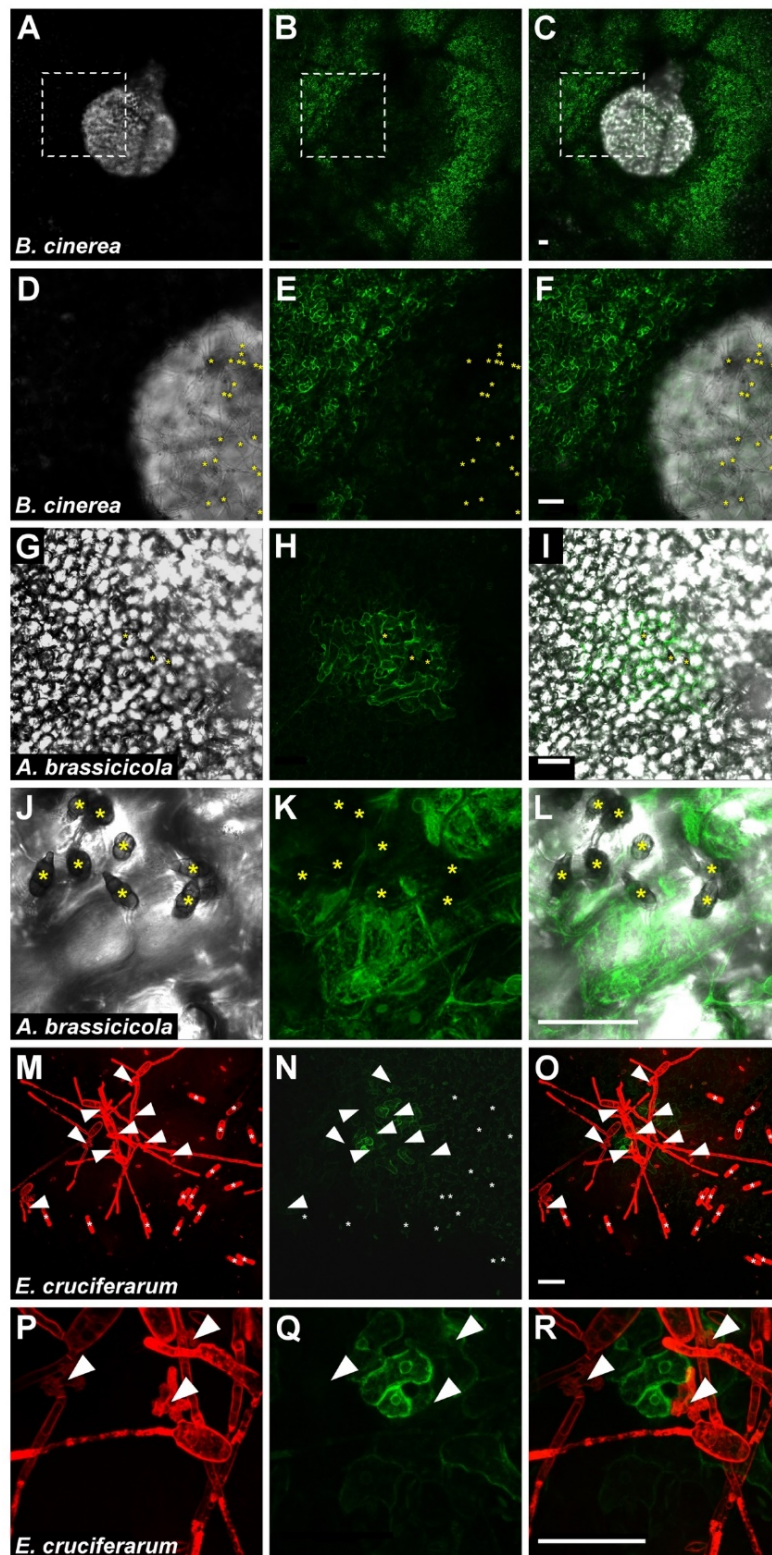


Figure 2: CYP71B15-GFP accumulates in cells surrounding fungal infection sites.

CYP71B15pro:CYP71B15-GFP expressing plants were inoculated with spores of *B. cinerea*, *A. brassicicola*, or *E. cruciferarum*, and expression of CYP71B15-GFP at fungal infections sites was detected. A-C: Site of infection with necrotrophic *B. cinerea* (central transparent leaf area) 24 hai. D-F: Higher magnification of the area indicated by the square in A-C. Asterisks indicate spores from which hyphae emerged. G-L: Sites of infection with *A. brassicicola* 18 hai. Asterisks indicate spores from which hyphae emerged. M-R: Sites of successful infection by the biotrophic powdery mildew fungus *E. cruciferarum* 24 hai. Arrowheads indicate sites of fungal attack/penetration; asterisks indicate non-germinated spores. The first column of pictures shows transmission channel images (A, D, G, J) or red staining of fungal structures after staining with FM4-64 (M, P), images in the second column show CYP71B15-GFP accumulation, and the third columns shows the overlay images of the two. Bars = 50 μ m.

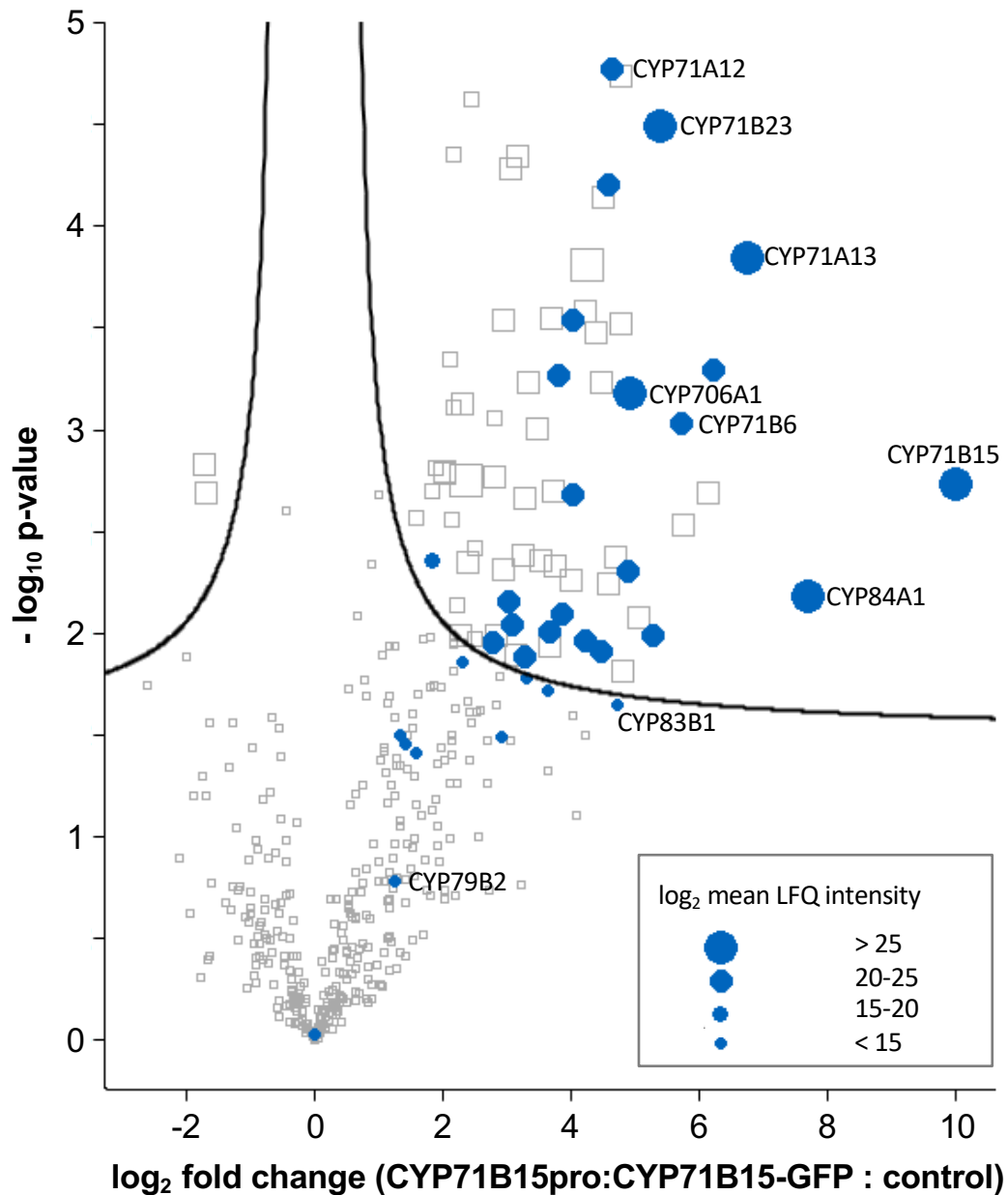


Figure 3: Proteins co-purified with CYP71B15-GFP from leaves infected with *B. cinerea*

CYP71B15-GFP was expressed under control of its endogenous promoter in the *pad3* background. The enrichment of interacting proteins in co-IP experiments (\log_2 fold change) is plotted against the significance of the change ($-\log_{10} p\text{-value}$). Cytochrome P450 enzymes, represented by blue circles, all other proteins by open squares and their respective size represents \log_2 Label-free quantification intensities (LFQ). P450 enzymes were strongly enriched including CYP71A13 and CYP71B6. P450 proteins above \log_2 LFQ intensity of 25 and those mentioned in the text are indicated. $n=3$.

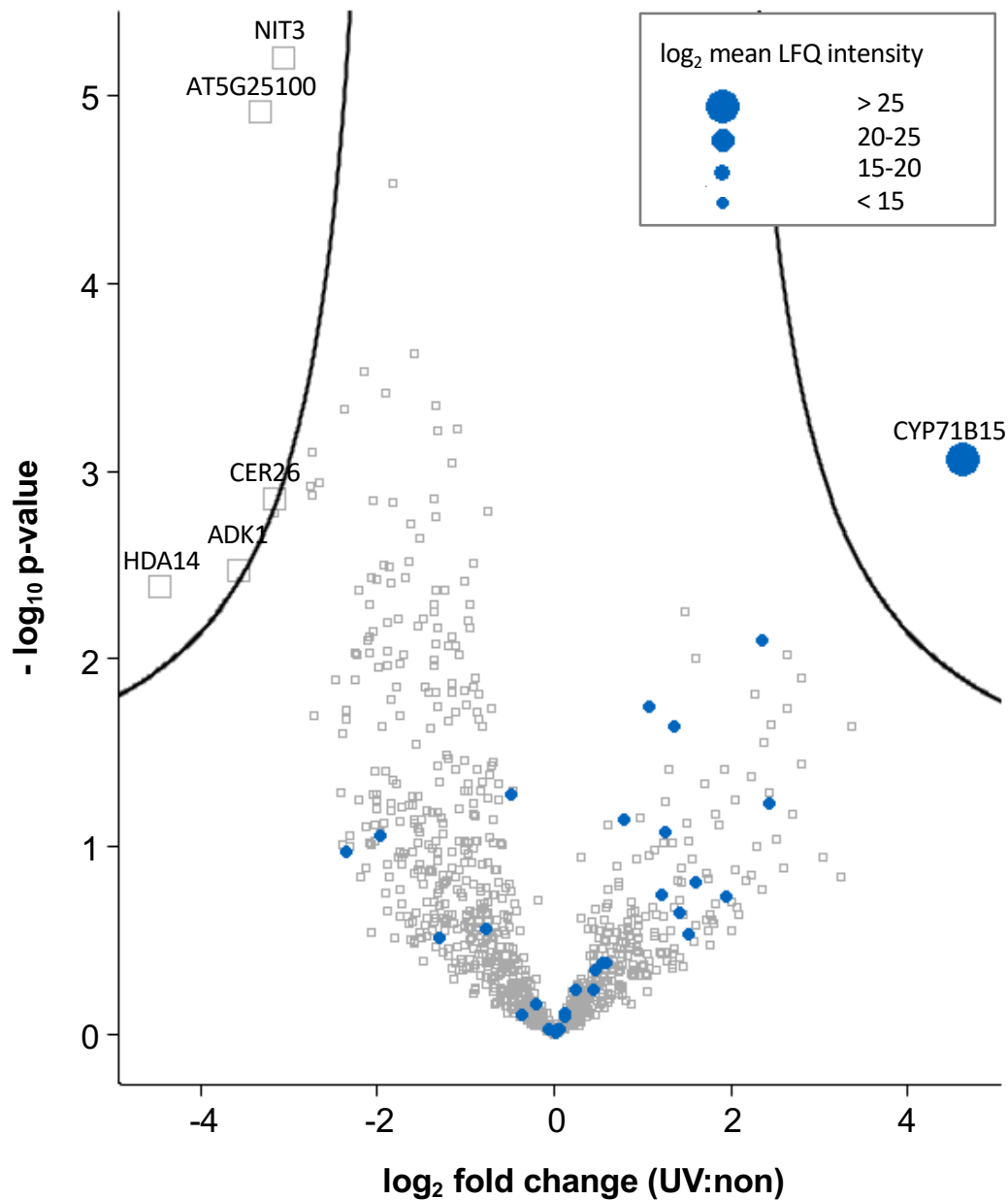


Figure 4: Proteins co-purified from leaves overexpressing CYP71A13-YFP with or without UV irradiation

The log₂ fold change (UV-irradiated versus untreated leaves) is plotted against the significance of the change ($-\log_{10}$ p-value). Cytochrome P450 enzymes, represented by blue circles, all other proteins by open squares and their respective size represents log₂ Label-free quantification intensities (LFQ). Named are proteins enriched significantly in UV or in control samples. UV-dependent co-purification of CYP71B15 was observed. n=3.

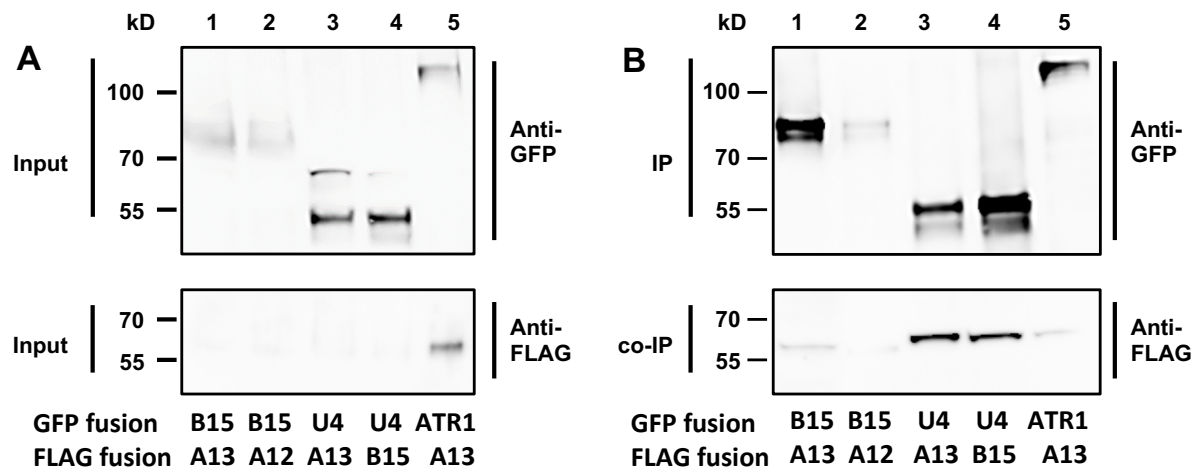


Figure 5: Co-IP analysis of the physical association of camalexin-specific enzymes

YFP and FLAG-tagged fusion proteins were transiently expressed in *N. benthamiana* and microsomal proteins were extracted four days after infiltration. Here, CYP71B15 (B15) in combination with CYP71A13 (A13) (1), CYP71A12 (A12) (2) or GSTU4 (U4) (4) and CYP71A13 in combination with GSTU4 (3) or ATR1 (5) **A**: Western blot analysis of input samples. **B**: Western Blot analysis on immunoprecipitation (IP) samples. IP was performed with anti-GFP antibody and interacting proteins were analysed with an anti-FLAG antibody. Interaction was shown for CYP71A13-FLAG with CYP71B15-YFP (1), GSTU4-YFP(3) and ATR1-YFP (5) and for CYP71B15-YFP with CYP71A12-FLAG (2) and GSTU4-FLAG (4). The experiment was repeated at least three times, with similar results. Combinations of fusion proteins, where no co-IP was observed are shown in Supplementary Figure 3.

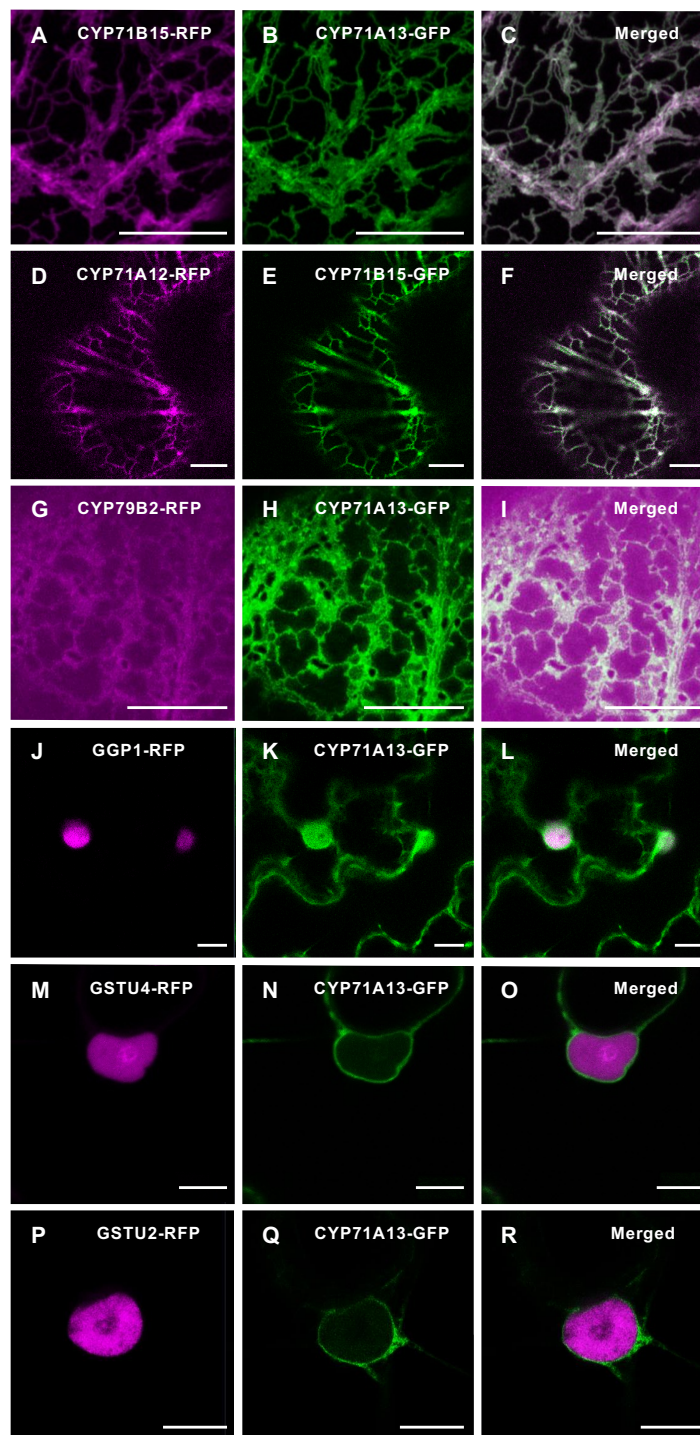


Figure 6: Co-localization of camalexin-specific enzymes in *N. benthamiana* leaves

In each case two GFP or RFP labelled P450 enzymes (A, B, D, E, G, H, K, N, Q) in different combinations or together with either GGP1-RFP (J), GSTU4-RFP (M) or GSTU2-RFP (P) were expressed transiently in *N. benthamiana* and analyzed for localization and co-localization three days after infiltration. Fluorescence signals for CYP71B15, CYP71A13, CYP71A12 and CYP79B2 fusion proteins were detected at the ER (A, B, D, E, G, H) with CYP79B2 expression levels substantially lower than the other proteins (G). GSTU4 (M) and GSTU2 (P) showed cytosolic localization indicated by the typical nuclear localization. Co-localization for CYP71A13 with CYP71B15 (C) and CYP79B2 (I) is shown in the merged images. Furthermore, CYP71B15 co-localizes with CYP71A12 (F) whereas no signal overlap is detectable when CYP71A13 is co-expressed with the cytosolic proteins GSTU4 (O) or GSTU2 (R) (see also Supplementary Fig. 4). Scale bar: 10 μ m

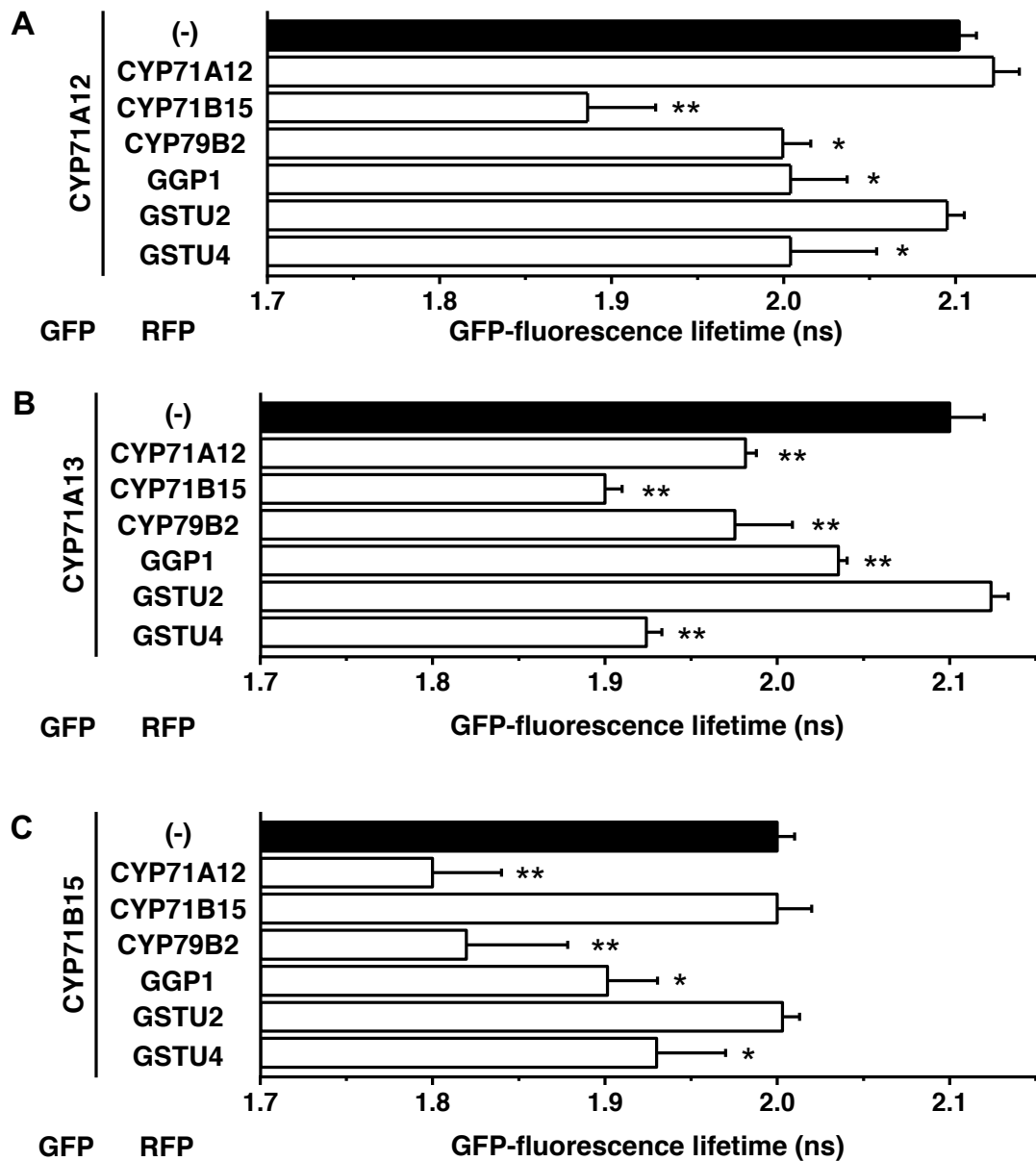


Figure 7: Tight physical interaction of camalexin-biosynthesis enzymes supported by Förster resonance energy transfer studies combined with fluorescence lifetime microscopy (FRET-FLIM)

GFP-tagged CYP71A12 (A), CYP71A13 (B) or CYP71B15 (C) was transiently expressed in *N. benthamiana* alone (black bars), or in combination with different RFP-tagged proteins (white bars). Three days after inoculation protein-protein interaction was determined by measuring the GFP-fluorescence lifetime via FLIM. In case of FRET a significant reduction of GFP-fluorescence lifetime was detectable compared to the donor only sample. Physical interaction could be observed for CYP71A12, CYP71A13, CYP71B15 with each other and with CYP79B2, GGP1, and GSTU4. No interaction with GSTU2 and no homodimerization of CYP71A12 or CYP71B15 was observed. Error bars indicate standard deviation of at least three independent replicates. One-way Anova for independent samples, standard weighted-means analysis, with Tukey's honestly significant difference (HSD) post hoc test; * $p < 0.05$; ** $p < 0.01$.

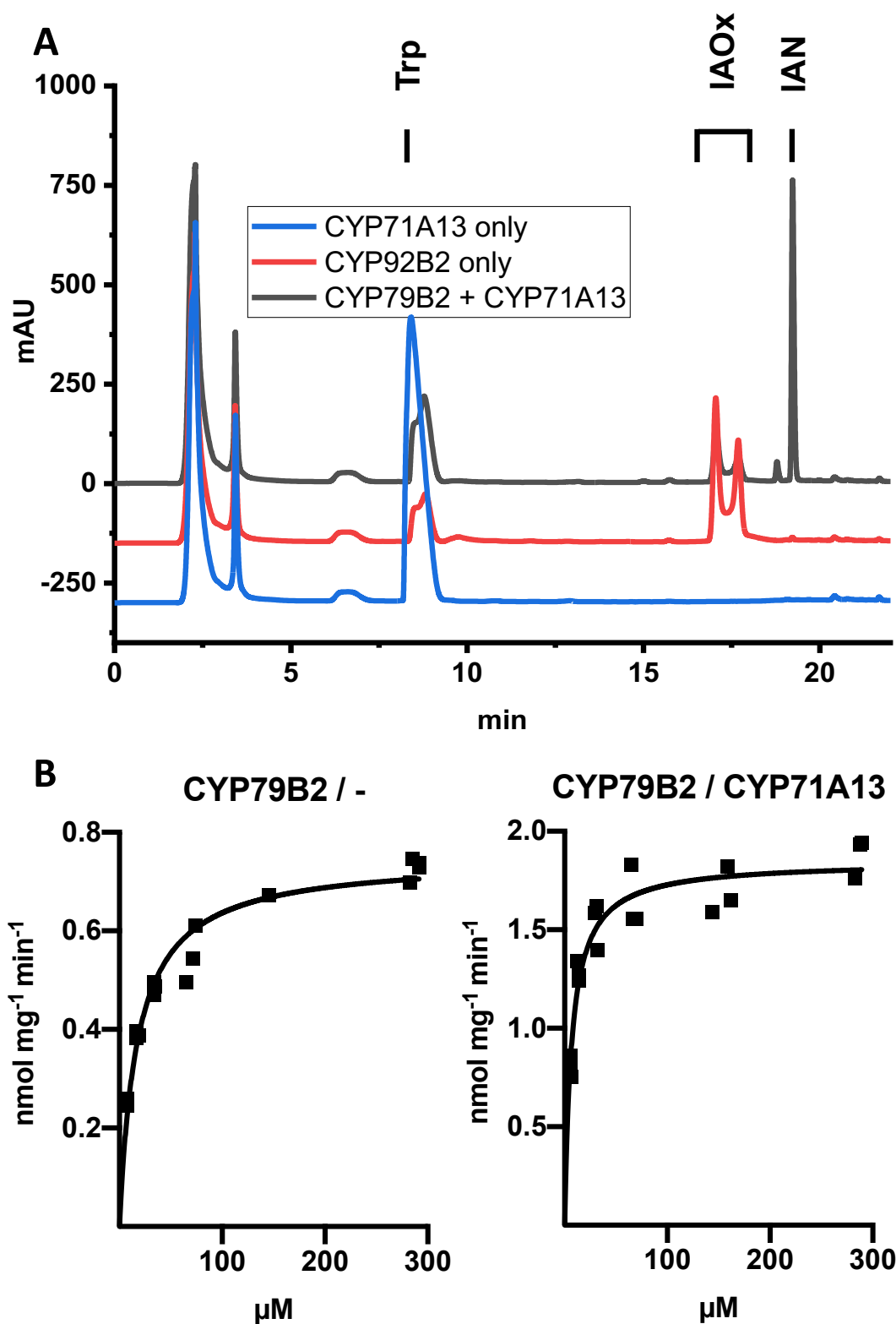
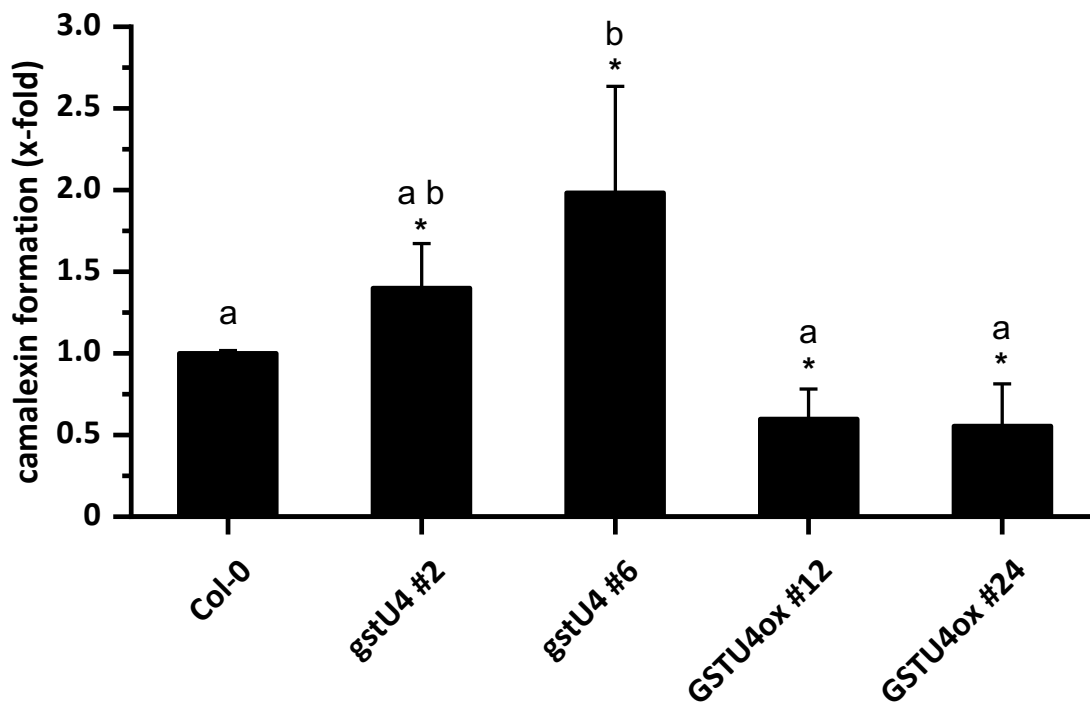


Figure 8: Higher apparent substrate affinity of CYP79B2 by presence of CYP71A13

CYP79B2 was expressed in *S. cerevisiae* together with CYP71A13 or vector control. **A**: Turnover of tryptophan with NADPH as co-substrate by corresponding microsomes; detection of substrate and products by HPLC; chromatogram at 278 nm. **B**: app. Km-value for tryptophan: CYP79B2: $K_m = 17.5 \pm 1.9 \mu\text{M}$, $R^2 = 0.95$; CYP79B2 / CYP71B13: $K_m = 6.9 \pm 0.9 \mu\text{M}$, $R^2 = 0.90$ (n=16).



1

Figure 9: Camalexin formation in response to *B. cinerea* infection in *gstu4* knockout and overexpression plants

Leaves of six-week-old plants were treated with *B. cinerea* spores. After 48 hours camalexin was extracted and levels were analyzed via HPLC. In *gstu4* lines camalexin level was significantly increased whereas a significant decrease was observed in GSTU4 overexpressing lines. Camalexin levels were shown as arithmetic mean with standard deviation of 27 independent plants. Different letters indicate significant differences according to ANOVA (Scheffé's test; $P < 0.05$); *: significant differences to Col-0 according to t-test ($P < 0.05$).

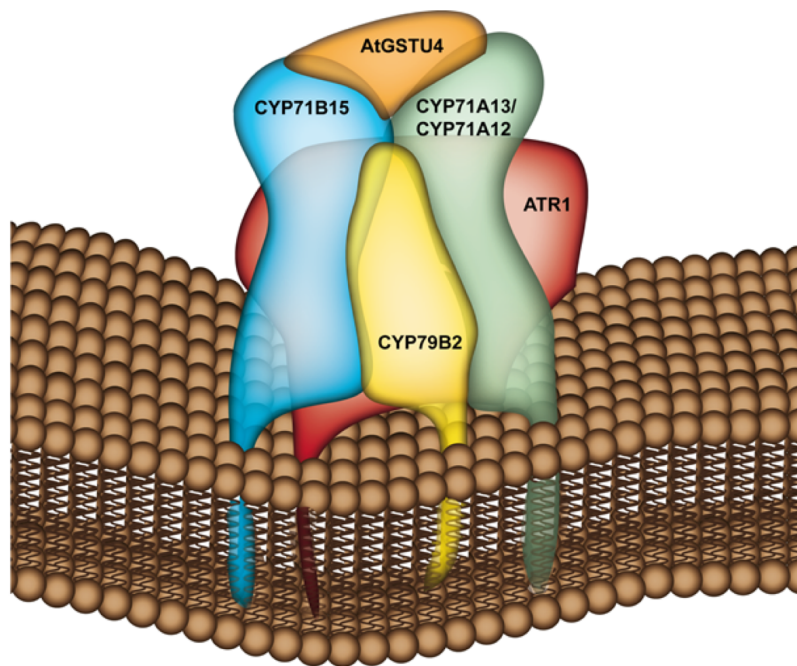


Figure 10: Model of a camalexin-biosynthetic metabolon

CYP79B2, CYP71A12/A13, CYP71B15 and ATR1 form a metabolic complex at the ER surface. CYP71B15 interacts with CYP79B2, CYP71A13 and CYP71A12 respectively. CYP79B2 is rather loosely associated to the complex and might function as a branch-point enzyme taking part in different protein complexes. Under stress conditions, the cytosolic component GSTU4 might be recruited to the complex. Its role in camalexin biosynthesis remains unsettled.

Parsed Citations

Adler, V., Yin, Z., Fuchs, S.Y., Benezra, M., Rosario, L., Tew, K.D., Pincus, M.R., Sardana, M., Henderson, C.J., and Wolf, C.R. (1999). Regulation of JNK signaling by GSTp. The EMBO journal 18, 1321-1334.

Pubmed: [Author and Title](#)

Google Scholar: [Author Only Title Only Author and Title](#)

Amberg, D.C., Burke, D.J., and Strathern, J.N. (2005). **Methods in Yeast Genetics: A Cold Spring Harbor Laboratory Course Manual, 2005 Edition (Cold Spring).**

Bak, S., Tax, F.E., Feldmann, K.A., Galbraith, D.W., and Feyereisen, R. (2001). CYP83B1, a cytochrome P450 at the metabolic branch point in auxin and indole glucosinolate biosynthesis in Arabidopsis. The Plant Cell 13, 101-111.

Pubmed: [Author and Title](#)

Google Scholar: [Author Only Title Only Author and Title](#)

Bak, S., Beisson, F., Bishop, G., Hamberger, B., Höfer, R., Paquette, S., and Werck-Reichhart, D. (2011). Cytochromes P450. The Arabidopsis Book, e0144.

Pubmed: [Author and Title](#)

Google Scholar: [Author Only Title Only Author and Title](#)

Bassard, J.E., Richert, L., Geerinck, J., Renault, H., Duval, F., Ullmann, P., Schmitt, M., Meyer, E., Mutterer, J., Boerjan, W., De Jaeger, G., Mely, Y., Goossens, A., and Werck-Reichhart, D. (2012). Protein-protein and protein-membrane associations in the lignin pathway. Plant Cell 24, 4465-4482.

Pubmed: [Author and Title](#)

Google Scholar: [Author Only Title Only Author and Title](#)

Becker, D., Kemper, E., Schell, J., and Masterson, R. (1992). New plant binary vectors with selectable markers located proximal to the left T-DNA border. Plant Molecular Biology 20, 1195-1197.

Pubmed: [Author and Title](#)

Google Scholar: [Author Only Title Only Author and Title](#)

Becker, W. (2012). Fluorescence lifetime imaging—techniques and applications. Journal of Microscopy 247, 119-136.

Pubmed: [Author and Title](#)

Google Scholar: [Author Only Title Only Author and Title](#)

Bednarek, P., Schneider, B., Svatoš, A., Oldham, N.J., and Hahlbrock, K. (2005). Structural complexity, differential response to infection, and tissue specificity of indolic and phenylpropanoid secondary metabolism in Arabidopsis roots. Plant Physiology 138, 1058-1070.

Pubmed: [Author and Title](#)

Google Scholar: [Author Only Title Only Author and Title](#)

Böttcher, C., Westphal, L., Schmotz, C., Prade, E., Scheel, D., and Glawischnig, E. (2009). The multifunctional enzyme CYP71B15 (PHYTOALEXIN DEFICIENT3) converts cysteine-indole-3-acetonitrile to camalexin in the indole-3-acetonitrile metabolic network of Arabidopsis thaliana. Plant Cell 21, 1830-1845.

Pubmed: [Author and Title](#)

Google Scholar: [Author Only Title Only Author and Title](#)

Böttcher, C., Chapman, A., Fellermeier, F., Choudhary, M., Scheel, D., and Glawischnig, E. (2014). The Biosynthetic Pathway of Indole-3-Carbaldehyde and Indole-3-Carboxylic Acid Derivatives in Arabidopsis. Plant Physiol 165, 841-853.

Pubmed: [Author and Title](#)

Google Scholar: [Author Only Title Only Author and Title](#)

Brachmann, C.B., Davies, A., Cost, G.J., Caputo, E., Li, J., Hieter, P., and Boeke, J.D. (1998). Designer deletion strains derived from Saccharomyces cerevisiae S288C: a useful set of strains and plasmids for PCR-mediated gene disruption and other applications. Yeast 14, 115-132.

Pubmed: [Author and Title](#)

Google Scholar: [Author Only Title Only Author and Title](#)

Brumos, J., Alonso, J.M., and Stepanova, A.N. (2014). Genetic aspects of auxin biosynthesis and its regulation. Physiologia Plantarum 151, 3-12.

Pubmed: [Author and Title](#)

Google Scholar: [Author Only Title Only Author and Title](#)

Chapman, A., Lindermayr, C., and Glawischnig, E. (2016). Expression of antimicrobial peptides under control of a camalexin-biosynthetic promoter confers enhanced resistance against Pseudomonas syringae. Phytochemistry 122, 76-80.

Pubmed: [Author and Title](#)

Google Scholar: [Author Only Title Only Author and Title](#)

Clough, S.J., and Bent, A.F. (1998). Floral dip: a simplified method for Agrobacterium-mediated transformation of Arabidopsis thaliana. Plant Journal 16, 735-743.

Pubmed: [Author and Title](#)

Google Scholar: [Author Only Title Only Author and Title](#)

Cobbett, C.S., May, M.J., Howden, R., and Rolls, B. (1998). The glutathione-deficient, cadmium-sensitive mutant, cad2-1, of Arabidopsis

thaliana is deficient in gamma-glutamylcysteine synthetase. Plant J 16, 73-78.

Pubmed: [Author and Title](#)

Google Scholar: [Author Only Title Only Author and Title](#)

Cox, J., and Mann, M. (2008). MaxQuant enables high peptide identification rates, individualized ppb-range mass accuracies and proteome-wide protein quantification. Nature Biotechnology 26, 1367.

Pubmed: [Author and Title](#)

Google Scholar: [Author Only Title Only Author and Title](#)

Cox, J., Neuhauser, N., Michalski, A., Scheltema, R.A., Olsen, J.V., and Mann, M. (2011). Andromeda: a peptide search engine integrated into the MaxQuant environment. Journal of Proteome Research 10, 1794-1805.

Pubmed: [Author and Title](#)

Google Scholar: [Author Only Title Only Author and Title](#)

Cox, J., Hein, M.Y., Lubner, C.A., Paron, I., Nagaraj, N., and Mann, M. (2014). Accurate Proteome-wide Label-free Quantification by Delayed Normalization and Maximal Peptide Ratio Extraction, Termed MaxLFQ. Molecular & Cellular Proteomics 13, 2513-2526.

Pubmed: [Author and Title](#)

Google Scholar: [Author Only Title Only Author and Title](#)

Crosby, K.C., Pietraszewski-Bogiel, A., Gadella, T.W., Jr., and Winkel, B.S. (2011). Forster resonance energy transfer demonstrates a flavonoid metabolite in living plant cells that displays competitive interactions between enzymes. FEBS Letters 585, 2193-2198.

Pubmed: [Author and Title](#)

Google Scholar: [Author Only Title Only Author and Title](#)

Czerniawski, P., and Bednarek, P. (2018). Glutathione S-Transferases in the Biosynthesis of Sulfur-Containing Secondary Metabolites in Brassicaceae Plants. Front Plant Sci 9, 1639.

Pubmed: [Author and Title](#)

Google Scholar: [Author Only Title Only Author and Title](#)

Dastmalchi, M., Bernards, M.A., and Dhaubhadel, S. (2016). Twin anchors of the soybean isoflavonoid metabolite: evidence for tethering of the complex to the endoplasmic reticulum by IFS and C4H. The Plant Journal 85, 689-706.

Pubmed: [Author and Title](#)

Google Scholar: [Author Only Title Only Author and Title](#)

Davydov, D.R., Davydova, N.Y., Sineva, E.V., and Halpert, J.R. (2015). Interactions among cytochromes P450 in microsomal membranes: oligomerization of cytochromes P450 3A4, 3A5, and 2E1 and its functional consequences. Journal of Biological Chemistry 290, 3850-3864.

Pubmed: [Author and Title](#)

Google Scholar: [Author Only Title Only Author and Title](#)

Dixon, D.P., Lapthorn, A., and Edwards, R. (2002). Plant glutathione transferases. Genome Biology 3, reviews3004. 3001.

Pubmed: [Author and Title](#)

Google Scholar: [Author Only Title Only Author and Title](#)

Förster, T. (1948). Zwischenmolekulare Energiewanderung und Fluoreszenz. Annalen der Physik 437, 55-75.

Pubmed: [Author and Title](#)

Google Scholar: [Author Only Title Only Author and Title](#)

Frerigmann, H., Pislewski-Bednarek, M., Sanchez-Vallet, A., Molina, A., Glawischnig, E., Gigolashvili, T., and Bednarek, P. (2016). Regulation of Pathogen-Triggered Tryptophan Metabolism in Arabidopsis thaliana by MYB Transcription Factors and Indole Glucosinolate Conversion Products. Mol Plant 9, 682-695.

Pubmed: [Author and Title](#)

Google Scholar: [Author Only Title Only Author and Title](#)

Fuchs, R., Kopischke, M., Klapprodt, C., Hause, G., Meyer, A.J., Schwarzlander, M., Fricker, M.D., and Lipka, V. (2016). Immobilized Subpopulations of Leaf Epidermal Mitochondria Mediate PENETRATION2-Dependent Pathogen Entry Control in Arabidopsis. The Plant cell 28, 130-145.

Pubmed: [Author and Title](#)

Google Scholar: [Author Only Title Only Author and Title](#)

Fujino, N., Tenma, N., Waki, T., Ito, K., Komatsuzaki, Y., Sugiyama, K., Yamazaki, T., Yoshida, S., Hatayama, M., Yamashita, S., Tanaka, Y., Motohashi, R., Denessiouk, K., Takahashi, S., and Nakayama, T. (2018). Physical interactions among flavonoid enzymes in snapdragon and torenia reveal the diversity in the flavonoid metabolite organization of different plant species. Plant J 94, 372-392.

Pubmed: [Author and Title](#)

Google Scholar: [Author Only Title Only Author and Title](#)

Gietz, D., St Jean, A., Woods, R.A., and Schiestl, R.H. (1992). Improved method for high efficiency transformation of intact yeast cells. Nucleic Acids Research 20, 1425.

Pubmed: [Author and Title](#)

Google Scholar: [Author Only Title Only Author and Title](#)

Glawischnig, E., Hansen, B.G., Olsen, C.E., and Halkier, B.A. (2004). Camalexin is synthesized from indole-3-acetaldoxime, a key branching point between primary and secondary metabolism in Arabidopsis. Proceedings of the National Academy of Sciences 101, 8245-8250.

Pubmed: [Author and Title](#)
Google Scholar: [Author Only Title Only Author and Title](#)

Glazebrook, J., and Ausubel, F.M. (1994). Isolation of phytoalexin-deficient mutants of *Arabidopsis thaliana* and characterization of their interactions with bacterial pathogens. *Proceedings of the National Academy of Sciences* 91, 8955-8959.

Pubmed: [Author and Title](#)
Google Scholar: [Author Only Title Only Author and Title](#)

Gronover, C.S., Kasulke, D., Tudzynski, P., and Tudzynski, B. (2001). The role of G protein alpha subunits in the infection process of the gray mold fungus *Botrytis cinerea*. *Mol Plant Microbe Interact* 14, 1293-1302.

Pubmed: [Author and Title](#)
Google Scholar: [Author Only Title Only Author and Title](#)

Hansen, C.H., Du, L., Naur, P., Olsen, C.E., Axelsen, K.B., Hick, A.J., Pickett, J.A., and Halkier, B.A. (2001). CYP83B1 is the oxime-metabolizing enzyme in the glucosinolate pathway in *Arabidopsis*. *Journal of Biological Chemistry* 276, 24790-24796.

Pubmed: [Author and Title](#)
Google Scholar: [Author Only Title Only Author and Title](#)

Hawes, C., and Kriechbaumer, V. (2018). *The Plant Endoplasmic Reticulum* (Springer).

Pubmed: [Author and Title](#)
Google Scholar: [Author Only Title Only Author and Title](#)

He, Y., Xu, J., Wang, X., He, X., Wang, Y., Zhou, J., Zhang, S., and Meng, X. (2019). The *Arabidopsis* Pleiotropic Drug Resistance Transporters PEN3 and PDR12 Mediate Camalexin Secretion for Resistance to *Botrytis cinerea*. *The Plant cell*.

Pubmed: [Author and Title](#)
Google Scholar: [Author Only Title Only Author and Title](#)

Julkowska, M., Koevoets, I.T., Mol, S., Hoefsloot, H.C., Feron, R., Tester, M., Keurentjes, J.J., Korte, A., Haring, M.A., and de Boer, G.-J. (2017). Genetic Components of Root Architecture Remodeling in Response to Salt Stress. *The Plant Cell*, tpc. 00680.02016.

Pubmed: [Author and Title](#)
Google Scholar: [Author Only Title Only Author and Title](#)

Karimi, M., De Meyer, B., and Hilson, P. (2005). Modular cloning in plant cells. *Trends in Plant Science* 10, 103-105.

Pubmed: [Author and Title](#)
Google Scholar: [Author Only Title Only Author and Title](#)

Katzen, F. (2007). Gateway® recombinational cloning: a biological operating system. *Expert Opinion on Drug Discovery* 2, 571-589.

Pubmed: [Author and Title](#)
Google Scholar: [Author Only Title Only Author and Title](#)

Kitamura, S., Shikazono, N., and Tanaka, A. (2004). TRANSPARENT TESTA 19 is involved in the accumulation of both anthocyanins and proanthocyanidins in *Arabidopsis*. *The Plant Journal* 37, 104-114.

Pubmed: [Author and Title](#)
Google Scholar: [Author Only Title Only Author and Title](#)

Klein, A.P., Anarat-Cappillino, G., and Sattely, E.S. (2013). Minimum Set of Cytochromes P450 for Reconstituting the Biosynthesis of Camalexin, a Major *Arabidopsis* Antibiotic. *Angewandte Chemie International Edition* 52, 13625-13628.

Pubmed: [Author and Title](#)
Google Scholar: [Author Only Title Only Author and Title](#)

Knudsen, C., Gallage, N.J., Hansen, C.C., Moller, B.L., and Laursen, T. (2018). Dynamic metabolic solutions to the sessile life style of plants. *Nat Prod Rep* 35, 1140-1155.

Pubmed: [Author and Title](#)
Google Scholar: [Author Only Title Only Author and Title](#)

Kowalski, N.A. (2016). Charakterisierung der Glutathiontransferasen aus *Arabidopsis thaliana*. In *Fakultät Wissenschaftszentrum Weihenstephan (Freising: TU-München)*, pp. 216.

Pubmed: [Author and Title](#)
Google Scholar: [Author Only Title Only Author and Title](#)

Krajewski, M.P., Kanawati, B., Fekete, A., Kowalski, N., Schmitt-Kopplin, P., and Grill, E. (2013). Analysis of *Arabidopsis* glutathione-transferases in yeast. *Phytochemistry* 91, 198-207.

Pubmed: [Author and Title](#)
Google Scholar: [Author Only Title Only Author and Title](#)

Kriechbaumer, V., Botchway, S.W., Slade, S.E., Knox, K., Frigerio, L., Oparka, K., and Hawes, C. (2015). Reticulomics: Protein-Protein Interaction Studies with Two Plasmodesmata-Localized Reticulon Family Proteins Identify Binding Partners Enriched at Plasmodesmata, Endoplasmic Reticulum, and the Plasma Membrane. *Plant Physiology* 169, 1933-1945.

Pubmed: [Author and Title](#)
Google Scholar: [Author Only Title Only Author and Title](#)

Kutz, A., Müller, A., Hennig, P., Kaiser, W.M., Piotrowski, M., and Weiler, E.W. (2002). A role for nitrilase 3 in the regulation of root morphology in sulphur-starving *Arabidopsis thaliana*. *The Plant Journal* 30, 95-106.

Pubmed: [Author and Title](#)
Google Scholar: [Author Only Title Only Author and Title](#)

Lallemand, B., Erhardt, M., Heitz, T., and Legrand, M. (2013). Sporopollenin biosynthetic enzymes interact and constitute a metabolon localized to the endoplasmic reticulum of tapetum cells. *Plant physiology* 162, 616-625.

Pubmed: [Author and Title](#)

Google Scholar: [Author Only](#) [Title Only](#) [Author and Title](#)

Laursen, T., Borch, J., Knudsen, C., Bavishi, K., Torta, F., Martens, H.J., Silvestro, D., Hatzakis, N.S., Wenk, M.R., and Dafforn, T.R. (2016). Characterization of a dynamic metabolon producing the defense compound dhurrin in sorghum. *Science* 354, 890-893.

Pubmed: [Author and Title](#)

Google Scholar: [Author Only](#) [Title Only](#) [Author and Title](#)

Lemarié, S., Robert-Seilaniantz, A., Lariagon, C., Lemoine, J., Marnet, N., Levrel, A., Jubault, M., Manzanares-Dauleux, M.J., and Grivot, A. (2015). Camalexin contributes to the partial resistance of *Arabidopsis thaliana* to the biotrophic soilborne protist *Plasmodiophora brassicae*. *Frontiers in plant science* 6.

Pubmed: [Author and Title](#)

Google Scholar: [Author Only](#) [Title Only](#) [Author and Title](#)

Mikkelsen, M.D., Hansen, C.H., Wittstock, U., and Halkier, B.A. (2000). Cytochrome P450 CYP79B2 from *Arabidopsis* catalyzes the conversion of tryptophan to indole-3-acetaldoxime, a precursor of indole glucosinolates and indole-3-acetic acid. *Journal of Biological Chemistry* 275, 33712-33717.

Pubmed: [Author and Title](#)

Google Scholar: [Author Only](#) [Title Only](#) [Author and Title](#)

Müller, T.M., Böttcher, C., and Glawischnig, E. (2019). Dissection of the network of indolic defence compounds in *Arabidopsis thaliana* by multiple mutant analysis. *Phytochemistry* 161, 11-20.

Pubmed: [Author and Title](#)

Google Scholar: [Author Only](#) [Title Only](#) [Author and Title](#)

Müller, T.M., Böttcher, C., Morbitzer, R., Götz, C.C., Lehmann, J., Lahaye, T., and Glawischnig, E. (2015). Transcription activator-like effector nuclease-mediated generation and metabolic analysis of camalexin-deficient *cyp71a12 cyp71a13* double knockout lines. *Plant Physiology* 168, 849-858.

Pubmed: [Author and Title](#)

Google Scholar: [Author Only](#) [Title Only](#) [Author and Title](#)

Nafisi, M., Goregaoker, S., Botanga, C.J., Glawischnig, E., Olsen, C.E., Halkier, B.A., and Glazebrook, J. (2007). *Arabidopsis* cytochrome P450 monooxygenase 71A13 catalyzes the conversion of indole-3-acetaldoxime in camalexin synthesis. *The Plant cell* 19, 2039-2052.

Pubmed: [Author and Title](#)

Google Scholar: [Author Only](#) [Title Only](#) [Author and Title](#)

Nintemann, S.J., Vik, D., Svozil, J., Bak, M., Baerenfaller, K., Burow, M., and Halkier, B.A. (2017). Unravelling protein-protein interaction networks linked to aliphatic and indole glucosinolate biosynthetic pathways in *Arabidopsis*. *Frontiers in Plant Science* 8.

Pubmed: [Author and Title](#)

Google Scholar: [Author Only](#) [Title Only](#) [Author and Title](#)

Nirenberg, H.I. (1981). A simplified method for identifying *Fusarium* spp. occurring on wheat. *Canadian Journal of Botany* 59, 1599-1609.

Pubmed: [Author and Title](#)

Google Scholar: [Author Only](#) [Title Only](#) [Author and Title](#)

Parisy, V., Poinssot, B., Owsianowski, L., Buchala, A., Glazebrook, J., and Mauch, F. (2007). Identification of PAD2 as a γ -glutamylcysteine synthetase highlights the importance of glutathione in disease resistance of *Arabidopsis*. *The Plant Journal* 49, 159-172.

Pubmed: [Author and Title](#)

Google Scholar: [Author Only](#) [Title Only](#) [Author and Title](#)

Perkins, J.R., Diboun, I., Dessailly, B.H., Lees, J.G., and Orengo, C. (2010). Transient protein-protein interactions: structural, functional, and network properties. *Structure* 18, 1233-1243.

Pubmed: [Author and Title](#)

Google Scholar: [Author Only](#) [Title Only](#) [Author and Title](#)

Rajniak, J., Barco, B., Clay, N.K., and Sattely, E.S. (2015). A new cyanogenic metabolite in *Arabidopsis* required for inducible pathogen defence. *Nature* 525, 376-379.

Pubmed: [Author and Title](#)

Google Scholar: [Author Only](#) [Title Only](#) [Author and Title](#)

Rauhut, T. (2009). Die Regulation der Camalexinbiosynthese in *Arabidopsis thaliana*. In *Lehrstuhl für Genetik* (Freising: TU-München).

Pubmed: [Author and Title](#)

Google Scholar: [Author Only](#) [Title Only](#) [Author and Title](#)

Rauhut, T., and Glawischnig, E. (2009). Evolution of camalexin and structurally related indolic compounds. *Phytochemistry* 70, 1638-1644.

Pubmed: [Author and Title](#)

Google Scholar: [Author Only](#) [Title Only](#) [Author and Title](#)

Reed, J.R., and Backes, W.L. (2012). Formation of P450·P450 complexes and their effect on P450 function. *Pharmacology & Therapeutics* 133, 299-310.

Pubmed: [Author and Title](#)
Google Scholar: [Author Only Title Only Author and Title](#)

Rothbauer, U., Zolghadr, K., Muyldermans, S., Schepers, A., Cardoso, M.C., and Leonhardt, H. (2008). A versatile nanotrapp for biochemical and functional studies with fluorescent fusion proteins. *Molecular & Cellular Proteomics* 7, 282-289.

Pubmed: [Author and Title](#)
Google Scholar: [Author Only Title Only Author and Title](#)

Schlaeppli, K., Abou-Mansour, E., Buchala, A., and Mauch, F. (2010). Disease resistance of *Arabidopsis* to *Phytophthora brassicae* is established by the sequential action of indole glucosinolates and camalexin. *The Plant Journal* 62, 840-851.

Pubmed: [Author and Title](#)
Google Scholar: [Author Only Title Only Author and Title](#)

Schoberer, J., and Botchway, S.W. (2014). Investigating protein-protein interactions in the plant endomembrane system using multiphoton-induced FRET-FLIM. *Methods in Molecular Biology* 1209, 81-95.

Pubmed: [Author and Title](#)
Google Scholar: [Author Only Title Only Author and Title](#)

Schuegger, R., Nafisi, M., Mansourova, M., Petersen, B.L., Olsen, C.E., Svatos, A., Halkier, B.A., and Glawischnig, E. (2006). CYP71B15 (PAD3) catalyzes the final step in camalexin biosynthesis. *Plant Physiology* 141, 1248-1254.

Pubmed: [Author and Title](#)
Google Scholar: [Author Only Title Only Author and Title](#)

Shevchenko, A., Tomas, H., Havli, J., Olsen, J.V., and Mann, M. (2006). In-gel digestion for mass spectrometric characterization of proteins and proteomes. *Nature Protocols* 1, 2856.

Pubmed: [Author and Title](#)
Google Scholar: [Author Only Title Only Author and Title](#)

Sønderby, I.E., Geu-Flores, F., and Halkier, B.A. (2010). Biosynthesis of glucosinolates—gene discovery and beyond. *Trends in plant science* 15, 283-290.

Pubmed: [Author and Title](#)
Google Scholar: [Author Only Title Only Author and Title](#)

Sparkes, I.A., Runions, J., Kearns, A., and Hawes, C. (2006). Rapid, transient expression of fluorescent fusion proteins in tobacco plants and generation of stably transformed plants. *Nature Protocols* 1, 2019-2025.

Pubmed: [Author and Title](#)
Google Scholar: [Author Only Title Only Author and Title](#)

Su, T.B., Xu, J.A., Li, Y.A., Lei, L., Zhao, L., Yang, H.L., Feng, J.D., Liu, G.Q., and Ren, D.T. (2011). Glutathione-Indole-3-Acetonitrile Is Required for Camalexin Biosynthesis in *Arabidopsis thaliana*. *Plant Cell* 23, 364-380.

Pubmed: [Author and Title](#)
Google Scholar: [Author Only Title Only Author and Title](#)

Sun, Y., Li, H., and Huang, J.-R. (2012). *Arabidopsis* TT19 Functions as a Carrier to Transport Anthocyanin from the Cytosol to Tonoplasts. *Molecular Plant* 5, 387-400.

Pubmed: [Author and Title](#)
Google Scholar: [Author Only Title Only Author and Title](#)

Tivendale, N.D., Ross, J.J., and Cohen, J.D. (2014). The shifting paradigms of auxin biosynthesis. *Trends in Plant Science* 19, 44-51.

Pubmed: [Author and Title](#)
Google Scholar: [Author Only Title Only Author and Title](#)

Toufighi, K., Brady, S.M., Austin, R., Ly, E., and Provart, N.J. (2005). The botany array resource: e-northerns, expression angling, and promoter analyses. *The Plant Journal* 43, 153-163.

Pubmed: [Author and Title](#)
Google Scholar: [Author Only Title Only Author and Title](#)

Tusher, V.G., Tibshirani, R., and Chu, G. (2001). Significance analysis of microarrays applied to the ionizing radiation response. *Proceedings of the National Academy of Sciences* 98, 5116-5121.

Pubmed: [Author and Title](#)
Google Scholar: [Author Only Title Only Author and Title](#)

Tyanova, S., and Cox, J. (2018). Perseus: A Bioinformatics Platform for Integrative Analysis of Proteomics Data in Cancer Research. In *Cancer Systems Biology* (Springer), pp. 133-148.

Pubmed: [Author and Title](#)
Google Scholar: [Author Only Title Only Author and Title](#)

Vizcaino, J.A., Côté, R.G., Csordas, A., Dianes, J.A., Fabregat, A., Foster, J.M., Griss, J., Alpi, E., Birim, M., and Contell, J. (2012). The PRoteomics IDentifications (PRIDE) database and associated tools: status in 2013. *Nucleic Acids Research* 41, D1063-D1069.

Pubmed: [Author and Title](#)
Google Scholar: [Author Only Title Only Author and Title](#)

Wagner, U., Edwards, R., Dixon, D.P., and Mauch, F. (2002). Probing the diversity of the *Arabidopsis* glutathione S-transferase gene family. *Plant Molecular Biology* 49, 515-532.

Pubmed: [Author and Title](#)

Google Scholar: [Author Only](#) [Title Only](#) [Author and Title](#)

Xu, J., Li, Y., Wang, Y., Liu, H., Lei, L., Yang, H., Liu, G., and Ren, D. (2008). Activation of MAPK kinase 9 induces ethylene and camalexin biosynthesis and enhances sensitivity to salt stress in Arabidopsis. Journal of Biological Chemistry 283, 26996-27006.

Pubmed: [Author and Title](#)

Google Scholar: [Author Only](#) [Title Only](#) [Author and Title](#)

Zhao, Y., Hull, A.K., Gupta, N.R., Goss, K.A., Alonso, J., Ecker, J.R., Normanly, J., Chory, J., and Celenza, J.L. (2002). Trp-dependent auxin biosynthesis in Arabidopsis: involvement of cytochrome P450s CYP79B2 and CYP79B3. Genes & Development 16, 3100-3112.

Pubmed: [Author and Title](#)

Google Scholar: [Author Only](#) [Title Only](#) [Author and Title](#)

Zhou, N., Tootle, T.L., and Glazebrook, J. (1999). Arabidopsis PAD3, a gene required for camalexin biosynthesis, encodes a putative cytochrome P450 monooxygenase. The Plant Cell 11, 2419-2428.

Pubmed: [Author and Title](#)

Google Scholar: [Author Only](#) [Title Only](#) [Author and Title](#)